Chapter 3

Spectroscopic and dielectric properties of ZnF_2-As_2O_3-TeO_2 glass system doped with V_2O_5

ZnF_2-As_2O_3-TeO_2 glasses mixed with different concentrations of V_2O_5 (ranging from 0 to 0.6 mol %) were synthesized. The amorphous nature of these glasses was checked by X-ray diffraction and scanning electron microscopy techniques. A variety of properties, i.e. optical absorption, photoluminescence, infrared, ESR spectra and dielectric properties (constant ε ', loss tan δ, ac conductivity σ_{ac} over a wide range of frequency and temperature) of these glasses have been explored. The optical absorption, electron spin resonance studies together indicated vanadium ions coexist in V^{4+} with V^{5+}state in the in these samples. The IR spectra of these samples have exhibited bands due to ν_s - TeO_{2ax} and AsO_3 structural groups; these results indicated the most structural disorder in the network as the concentration of V_2O_5 is increased. Luminescent emission spectra recorded at room temperature of these glasses excited at 640 nm have exhibited a broad emission band in the spectral wavelength range of 750-850 nm. The luminescence efficiency is found to be the highest for the sample doped with 0.6 mol%. The dielectric parameters viz., ε', $\tan\delta$ and $\sigma_{a.c}$ are found to increase and the activation energy for ac conduction is found to decrease with the increase in the concentration of V_2O_5 up to 0.6 mol%, reflecting an increase in the concentration of V^{4+} ions that take part modifying positions in the glass network. The ac conduction in these glasses could satisfactorily be explained by both classical activation energy and the tunneling phenomena.

Spectroscopic and dielectric properties of ZnF_2–As_2O_3–TeO_2 glass system doped with V_2O_5

3.1 Introduction

Tellurium oxide is an incipient glass network former and as such does not form the glass. Hence the addition of strong network former like As_2O_3 to tellurium oxide glasses improve the glass forming ability and the optical transparency in the blue as well as in the IR regions [1]. As_2O_3 is the only strong network former besides GeO_2 that exhibit significant transmission potential farther into the infrared. This is illustrated by calculated wavelength of λ_o, the material dispersion crossover point which is 1.3 μm for P_2O_5, B_2O_3 and SiO_2, 1.7 μm for GeO_2 and 1.9 μm for As_2O_3 [2, 3]. The addition of As_2O_3 is expected to affect the infrared transmission of TeO_2 glasses to a less extent, since the frequencies of some of the fundamental modes of vibration of As_2O_3 structural groups lay in the region of vibrations of TeO_4 structural groups [3]. In view of this, it is also predicted that AsO_3 groups form a single arsenic–tellurium–oxygen framework with the TeO_4 structural units and may strengthen the glass network. Addition of the modifier like ZnF_2 to TeO_2–As_2O_3 glass matrix is expected to lower the viscosity and to decrease the liquidus temperature to a substantial extent and makes the glass more moisture resistant [4].

Semiconducting transition metal oxide (like V_2O_5) mixed glasses have gained importance in recent years due to their possible applications in various technological fields [5–7]. Among various semiconducting transition metal oxide glasses, the vanadate glasses find applications in memory and switching devices. The glasses containing vanadium ions have also attracted much interest in solid-state chemistry and materials science. V_2O_5 is known to participate in the glass network with VO_5 pyramidal structural units. Several vanadate glasses show semiconducting behavior with the electrical conductivity of 10^{-3} to 10^{-5} $(ohm–cm)^{-1}$, which is known to be due to electron hopping between V^{4+} to V^{5+} ions, existing in the glass network. More precisely, vanadium ion containing glasses are identified as the n-type semiconductors for low value of the V^{4+}/V^{5+} ratio. The process of hopping of the electrons between V^{4+} and V^{5+} ions in the presence of larger concentrations of mobile cations, is highly interesting and useful to investigate. Though, a considerable number of recent studies on vanadium ions doped glass systems including some TeO_2 are available [8–10], most of them are restricted to dc conductivity studies. Studies available on spectroscopic (including photoluminescence) and dielectric properties of V_2O_5 doped tellurite glasses are very few and still there is a lot of scope to probe vanadium ion in tellurite glasses especially when they are mixed with strong glass network former like As_2O_3. Further, the results of dielectric measurements together with

spectroscopic studies may also throw some light on many aspects, such as the geometry of structural units of glass network, the character of chemical bonds of vanadium ions. The objective of this chapter is to have a comprehensive understanding over the topology and valence states of vanadium ions in $20ZnF_2–30As_2O_3–(50–x)TeO_2$: xV_2O_5 ($0 \leq x \leq 0.6$) glass network by a systematic study of dielectric properties over a wide range of frequency and temperature and spectroscopic properties (viz., optical absorption, photoluminescence, ESR and IR) studies.

3.2 Brief review of the previous work on the glasses containing vanadium ions

The studies as such on vanadium containing tellurite glasses are limited. However in this review, the studies on different glass systems including some tellurite glasses containing vanadium ions, has been described briefly.

Kerkouri *et al.* [11] have reported spectroscopic studies and the structural aspects of V_2O_5-CdO-P_2O_5 glasses. In their study it was reported that the glasses containing more than 20% of V_2O_5, the VO_4 and VO_5 structural units with V–O–V bridges were formed in the glass network. Lin-Hua *et al.* [12] have recently reported electron paramagnetic resonance spectra of vanadyl doped zinc phosphate glass. In this study the compressed defect structure of V^{4+} center is discussed in detail. Gouda *et al.* [13] have investigated the effect of replacing vanadium by Cu^{2+} ion on the dc-electrical conductivity (σ) and I–V characteristics of $(V_2O_5)_{0.7}(GeO_2)_{0.3}(CuO)_x$ glasses. In this report the

electrical conduction is interpreted on the basis of electrons hopping from reduced to unreduced vanadium and/or cupper ions. Ali and Ezz-Eldin [14] have studied some physical properties of the lithium disilicate ($Li_2Si_2O_5$) glasses doped with different ratios of V_2O_5 before and after gamma-rays irradiation. The observed variations in the physical properties with the change in the concentration of V_2O_5 were correlated with the changes in internal glass network. Abd El-Aal and Afifi [15] have reported the elastic properties of vanadium tellurite glasses, $65TeO_2–(35\text{-}x)V_2O_5–xCUO$, with different compositions of copper at room temperature by ultrasonic methods. Agarwal *et al.* [16] have recently reported the electron paramagnetic resonance studies of vanadyl doped alkali niobium borate glasses. In this study it was observed that the tetragonality of $V^{4+}O_6$ complex decreases with increasing concentration of Nb_2O_5. Khattak *et al.* [17] have studied X-ray photoelectron spectroscopy (XPS) and magnetic susceptibility studies of vanadium phosphate glasses. From the analysis of the results of these studies, the authors have proposed a glass structure model consisting of a mixture of vanadate phosphate phases that include V_2O_5, $VOPO_4$, $(VO)_2P_2O_7$, $VO(PO_3)$, and $V(PO_3)_3$ with the abundance of orthophosphate $(PO_4)^{3-}$ units increasing with increasing vanadium content. In another report [18] these authors have also reported the results of X-ray photoelectron spectroscopy (XPS) of vanadium tellurite glasses. Quantitative analysis of the results of these studies has indicated that there is a change of

TeO_4 tbp to TeO_3 tp upon V_2O_5 addition. Behzad *et al.* [19] have studied the conductivity of $50P_2O_5–xV_2O_5–(50–x)Li_2O$ glass system as a function of temperature and composition. Isothermal variation of conductivity as a function of composition of this study showed a minimum for a molar ratio x near 20. Probable mechanisms for decrease of conductivity with decrease of vanadium oxide concentration were explained in detail.

Saddeek [20] has recently reported FTIR and elastic properties by ultrasonic methods on $MoO_3–V_2O_5–PbO$ glasses. The observed compositional dependence of the elastic moduli was interpreted in terms of the effect of MoO_3 on the coordination number of the vanadate units. A good correlation was observed between the experimentally determined elastic moduli and those computed according to the Makishima-Mackenzie model. Shapaan *et al.* [21] have investigated hyperfine structure and electric transport properties of vanadium iron phosphate glasses and interpreted the results with the aid of the data on Mössbauer spectroscopy. Increase of V_2O_5 content, resulted the increase in dc conductivity while the activation energy was found to decrease. The observed increase of dielectric constant $\varepsilon'(\omega)$ with increasing V_2O_5 content was attributed to the increase in the deformation of glass network. Feng [22] has reported detailed theoretical studies of the optical and EPR spectra for vanadyl ions in alkaline-earth aluminoborate glasses. In this study the Optical spectra and electron paramagnetic resonance (EPR), g and A factors of calcium

aluminoborate glasses (CaAB): VO^{2+} are calculated using a complete diagonalization (of the energy matrix) process. Good agreement between the theoretical values and experimental results attributed effectiveness of the CDP method for theoretical studies of optical and EPR spectra of $3d^1$ (or V^{4+}) ions in glasses. Bogomolova *et al.* [23] have reported electron paramagnetic resonance studies of V^{4+} ions in lanthanum-aluminosilicate glasses. From the detailed analysis of EPR spectra it was concluded that in the samples containing low content of La_2O_3 lanthanum acts predominately as modifying ion where as in glass with a high La_2O_3 concentration lanthanum gradually occupies a glass forming site in the network. Kartashov and Vysloukh [24] have investigated the propagation of laser beams in $SiO^{2-}VO_2$ nanocomposite waveguides with thermo-optical nonlinearity. These studies have indicated that the large modifications of the absorption coefficient as well as notable changes of the refractive index of VO_2 nanoparticles embedded into the SiO_2 host media that accompany the semiconductor-to-metal phase transition. At the end they have concluded that such changes may lead to optical limiting in the near-IR wave range.

Kim *et al.* [25] have investigated the local structures of the boron and vanadium sites in the ternary $xV_2O_5–B_2O_3–yNa_2O$ glass by means of magic angle spinning (MAS) nuclear magnetic resonance (NMR) techniques. In this study it was observed that with increasing x, the mole ratios of the BO_3 and

BO_4 structures were enhanced, as were the quadrupole asymmetry parameters for the BO_3 structures, while the quadrupole coupling constants for the sites were reduced. Sung *et al.* [26] have investigated a variety of thermal properties of P_2O_5–V_2O_5–ZnO/B_2O_3 glasses that include glass transition temperature, dilatometer softening point and coefficient of thermal expansion, and aqueous durability. From these studies it was observed that the aqueous durability was improved through the addition of some additives such as Al_2O_3 and TiO_2. Moawad *et al.* [27] have investigated dc conductivity the mixed electronic-ionic conduction in $0.5[xAg_2O–(1–x)V_2O_5]–0.5TeO_2$ glasses. In this study it was observed that the mechanism of dc conductivity changes from predominantly electronic to ionic within the $30 \leq Ag_2O \leq 40$ range. Taibi *et al.* [28] have investigated the influence of the V_2O_5/Sb_2O_3 substitution on the physical properties of the $(70–x)Sb_2O_3–xV_2O_5–30K_2O$ glasses. From these studies the authors have suggested that there is a change in the coordination number of the vanadium cations in relation to the network topology. ElBatal *et al.* [29] have prepared V_2O_5-doped sodium phosphate glasses of various compositions and studied various spectroscopic properties that include UV-vis and infrared, Raman and electron spin resonance. In this study the changes observed in UV-vis and infrared spectral data were discussed in relation to the structural evolution caused by the change in the V_2O_5 content or glass composition. Farah [30] has studied the relationship between glass composition

and optical basicity by redox analysis of vanadium in Na_2O and CaO based Al_2O_3–SiO_2 glasses/melts. In this study it was found that the V^{4+}/V^{5+} equilibrium was more affected by a change in the calculated optical basicity compared with that of the V^{3+}/V^{4+} in both sodium and calcium silicate series. However, Alumina saturation from the crucible did not affect the calculated optical basicity of the sodium silicate glasses, although there was a change in the corresponding redox ratios. The results were compared using different experimental parameters and were found to be useful in glass production and extractive metallurgy of vanadium.

Kumar *et al.* [31] have reported thermal and electrical properties of tellurium-based glasses doped with vanadium and vanadium-cobalt oxides. From the thermal properties the authors have estimated that the thermal stability, fragility and glass-forming tendency of the glass system. The results of dc conductivity have been analyzed in the light of Mott's small polaron hopping (SPH) and Mott's and Greave's variable range hopping (VRH) models. Vedeanu *et al.* [32] have investigated structural changes induced by CuO and V_2O_5 in the phosphate glass network by means of Raman spectroscopy. In this study it was observed that at higher concentrations of V_2O_5 a strong depolymerization of the phosphate network was taking place. Kundu *et al.* [33] have investigated effect of V_2O_5 on structural, physical and electrical properties of bismuth borate glasses. In this study the dc conduction was found

to increase with increase in vanadium content and the mechanism was explained in terms of polaron hopping. Rao *et al.* [34] have reported dielectric dispersion in $Li_2O–MoO_3–B_2O_3$ glass system doped with V_2O_5. The observed dielectric relaxation effect was analyzed quantitatively by pseudo Cole-Cole plot method and the spreading of relaxation times was established. Rada *et al.* [35] have investigated the effect of the introduction of vanadium pentaoxide on structural changes in phospho-tellurite glasses containing gadolinium ions. In these studies it was found that the addition of V_2O_5 resulted in gradual depolymerization of the phosphate chains and formation of short phosphate units in the glass network. Li *et al.* [36] have studied the effect of lanthanum on structure of vanadate-phosphate glass by means of Fourier infrared spectroscopy, Raman spectroscopy and nuclear magnetic resonance. The analysis of these results have indicated that vanadium existed in the glass in the form of $(VO_3)_n$ single chains, $(V_2O_8)_n$ zigzag chains, VO_4 branches and groups.

Al-Assiri [37] has studied electrical properties of vanadium-copper-phosphate glasses. In this study the dc conductivity was found to increase while the activation energy is found to decrease with the increase of the V_2O_5 content. Further, it was reported that the dc conductivity in these glasses is electronic in nature and depends strongly upon the average distance, R, between the vanadium ions. Tian *et al.* [38] have investigated the effect of V_2O_5 content on the phase-transformation and the microstrctural development

in the SiO_2–MgO–Al_2O_3–K_2O–V_2O_5–F glass by XRD, SEM and EPMA measurements. In this study it was found that the incorporation of V_2O_5 leads to the precipitation of mullite ($Al_6Si_2O_{13}$) crystalline phases at lower temperatures. Further, it was reported that although the types of crystalline phases, which are formed as mullite and mica, were less influenced by V_2O_5 contents, the morphology, volume fraction and sizes of crystals were dependent sensitively on the V_2O_5 content. Hager [39] has reported the region of glass formation of ternary V_2O_5–BaF_2–RF (RF=LiF, NaF and mixed NaF–LiF) and has also measured a variety of physical parameters that include density, molar volume, characteristic temperatures, average thermal expansion coefficient, α, and specific heat, C_p. In this study it was observed that the glass-transition temperature, T_g, decreased by increase of RF while thermal expansion, α, and specific heat, C_p, near T_g were increased. Ardelean *et al.* [40] reported the EPR study of V_2O_5–P_2O_5–Li_2O glass system. In this study it was found that at high V_2O_5 content, the vanadium hyperfine structure disappears and only the broad line could be observed in the spectra. Spin Hamiltonian parameters $g_{\|}$, $g_{\perp}$ $A_{\|}$, $A_{\perp}$, dipolar hyperfine coupling parameters, P, and Fermi contact interaction parameters, K, have been calculated. The composition dependence of line widths of the first two absorptions from the parallel band and of the broad line characteristic to the cluster formations was also discussed in detail.

Mekki *et al.* [41] have investigated the magnetic properties of vanadium-sodium silicate glasses. Ferrari *et al.* [42] have probed the effect of V_2O_5 on the crystallization of $CaO–ZrO_2–SiO_2$ glasses. Abd El-Moneim [43] has carried out DTA and IR spectra of vanadium tellurite glasses. Hoppe *et al.* [44] have reported the details on structure of vanadium tellurite glasses by using neutron and X–ray diffraction. Cozar *et al.* [45] have studied the IR and EPR studies on some lithium borate glasses with vanadium ions. Salim *et al.* [46] have carried out X–ray photoelectron spectroscopy and magnetization studies of iron–vanadium phosphate glasses. Khattak *et al.* [47] have studied X–ray photoelectron spectroscopy (XPS) and magnetic properties of copper-vanadium phosphate glasses. Jung *et al.* [48] have carried out NMR investigations on $PbO–B_2O_3$ glasses containing V_2O_5 and they have calculated the ratio of BO_4 and BO_3 units as a function of V_2O_5 concentration. Krasowski *et al.* [49] have measured electrical conductivity of silver vandate glasses. Maria-Camelja *et al.* [50] have investigated the ionic and electronic conductivity of $P_2O_5–V_2O_5–Na_2O$ glasses.

Mori *et al.* [51] have discussed the conduction phenomenon in $V_2O_5–Sb–TeO_2$ glasses on the basis of small polaron hopping model. Rajendran *et al.* [52] have carried out ultrasonic investigations in $V_2O_5–PbO$ glasses containing $BaTiO_3$. Simockova *et al.* [53] have investigated complex impedance response of $V_2O_5–P_2O_5$ glasses. Sudarsan *et al.* [54] have carried out a study on the

structural aspects of V_2O_5–P_2O_5–B_2O_3 glasses by using MAS NMR and IR spectral studies. Sega *et al.* [55] have studied the electrical conduction in V_2O_5–NiO–TeO_2 glasses. Moustafa *et al.* [56] have reported the spectroscopic studies of semiconducting barium vandate glasses doped with iron oxide. Attos *et al.* [57] have investigated the structure of borovanadate glasses by Raman spectroscopy. Murawski *et al.* [58] has investigated the dielectric relaxation in semiconducting glasses. Seth *et al.* [59] have studied the EPR study of vanadyl ion in CoO–PbO–B_2O_3 glasses. Takahashi *et al.* [60] have investigated the structure of AgI–Ag_2O–V_2O_5 glasses. Prakash *et al.* [61] have carried out the EPR study of vanadyl ion in CoO-PbO-B_2O_3 glasses. Bogomolova *et al.* [62] have investigated the role of V_2O_5 on the structure of fluoro germanate glasses using ESR measurements. Yoko *et al.* [63] have studied the IR and NMR spectral studies on lead vanadate glasses. Ghosh *et al.* [64] have reported the spectral studies of binary iron vanadate glasses. Gupta *et al.* [65] reported the influence of V^{4+} ion concentration on the EPR spectra of vanadate glasses. Adams *et al.* [66] have studied the silver ion conductivity during the crystallization of AgI–Ag_2O–V_2O_5 glasses. Dimitrov *et al.* [67] have analyzed V_2O_5–GeO_2–Bi_2O_3 glass structure by IR spectra. Amano *et al.* [68] have studied the electrical properties of Sb_2O_3–CaO–V_2O_5 glasses and glass ceramics.

3.3 Results

For the present study a particular composition viz., $20ZnF_2–30As_2O_3–(50–x)TeO_2: xV_2O_5$ (with x ranging from 0 to 0.6) is chosen. The details of the composition are:

V_0: $20ZnF_2–30As_2O_3–50TeO_2$

V_1: $20ZnF_2–30As_2O_3–49.9TeO_2: 0.1V_2O_5$

V_2: $20ZnF_2–30As_2O_3–49.8TeO_2: 0.2V_2O_5$

V_3: $20ZnF_2–30As_2O_3–49.7TeO_2: 0.3V_2O_5$

V_4: $20ZnF_2–30As_2O_3–49.6TeO_2: 0.4V_2O_5$

V_5: $20ZnF_2–30As_2O_3–49.5TeO_2: 0.5V_2O_5$

V_6: $20ZnF_2–30As_2O_3–49.4TeO_2: 0.6V_2O_5$

From the measured values of density d and calculated average molecular weight $\overline{M}$, various physical parameters such as vanadium ion concentration N_i and mean vanadium ion separation r_i of these glasses are evaluated using the conventional formulae and are presented in Table 3.1.

The SEM pictures (Fig. 3.1) and X–ray diffraction pattern (Fig. 3.2) of the $ZnF_2–As_2O_3–TeO_2: V_2O_5$ samples indicated virtually no crystallinity. The chemical makeup of the glasses is evaluated using EDS (Fig. 3.3); the EDS analysis indicates the presence of Te, Zn, O, F, As and V elements in the glass samples.

Table 3.1. Summary of data on various physical parameters of ZnF_2–As_2O_3–TeO_2 glasses.

Glass	Conc. V_2O_5 (mol%)	Avg. Mol. Wt. $\overline{M}$	Density (g/cm^3)	Total vanadium ion conc. N_i (10^{21} /cm^3)	Inter ionic dist.of vanadyl ions r_i (A^o)	Polaron radius r_p (A^o)
V_0	0	159.83	5.304	-	-	-
V_1	0.1	159.85	5.299	2.00	7.94	3.20
V_2	0.2	159.87	5.295	3.99	6.31	2.54
V_3	0.3	159.89	5.288	5.98	5.51	2.22
V_4	0.4	159.92	5.283	7.96	5.01	2.02
V_5	0.5	159.94	5.277	9.94	4.65	1.87
V_6	0.6	159.96	5.269	11.9	4.38	1.76

Fig. 3.4 represents differential scanning calorimetric (DSC) scan of ZnF_2–As_2O_3–TeO_2 glass doped with 0.3 mol% V_2O_5. The trace has exhibited an endothermic effect due to glass transition at about 295 ^oC followed by a well–defined exothermic effect due to crystallization temperature (T_C). The trace also exhibited another endothermic effect due to melting temperature at 570 ^oC. The DSC scans for other glasses have exhibited the similar behaviour. The variation of glass transition temperature (T_g) and glass forming ability parameter (K_{gl}) with concentration of V_2O_5 are shown as inset of Fig. 3.4. These parameters have been observed to decrease with the concentration of V_2O_5.

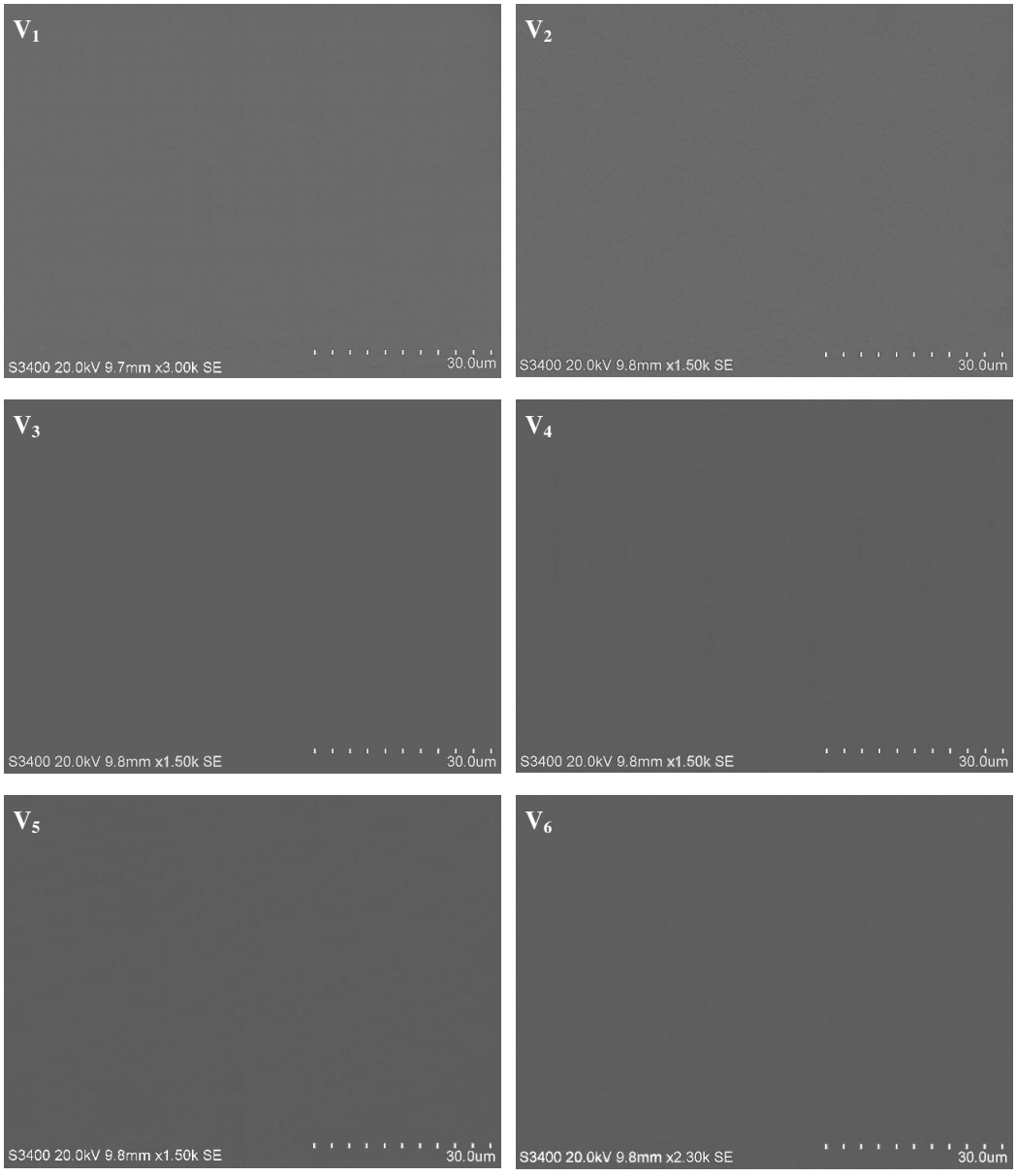

Fig. 3.1 SEM pictures of ZnF_2–As_2O_3–TeO_2: V_2O_5 glasses.

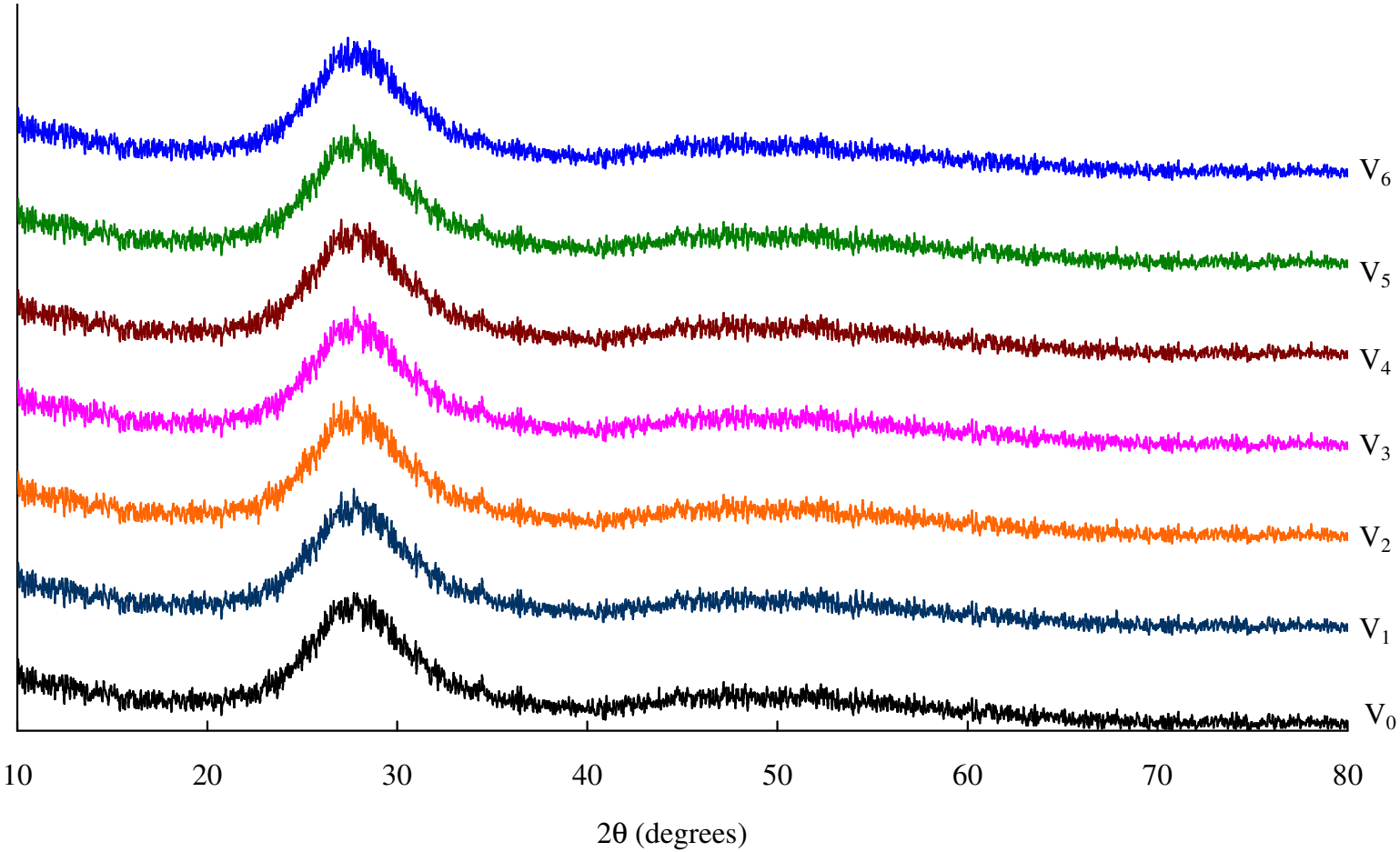

Fig. 3.2 X-ray diffraction pattern of ZnF_2–As_2O_3–TeO_2: V_2O_5 glasses.

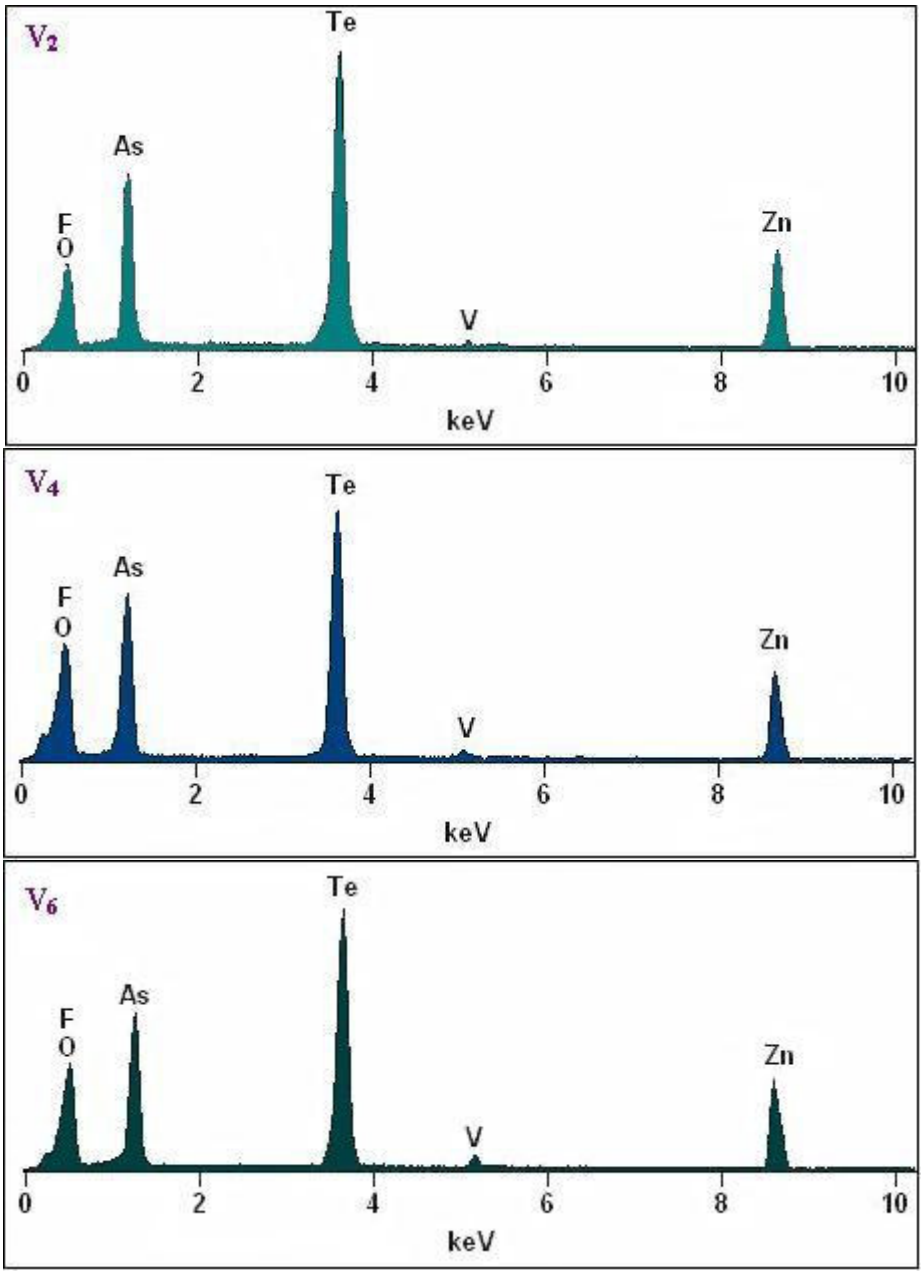

Fig. 3.3 EDS pictures of some of the ZnF_2–As_2O_3–TeO_2: V_2O_5 glasses.

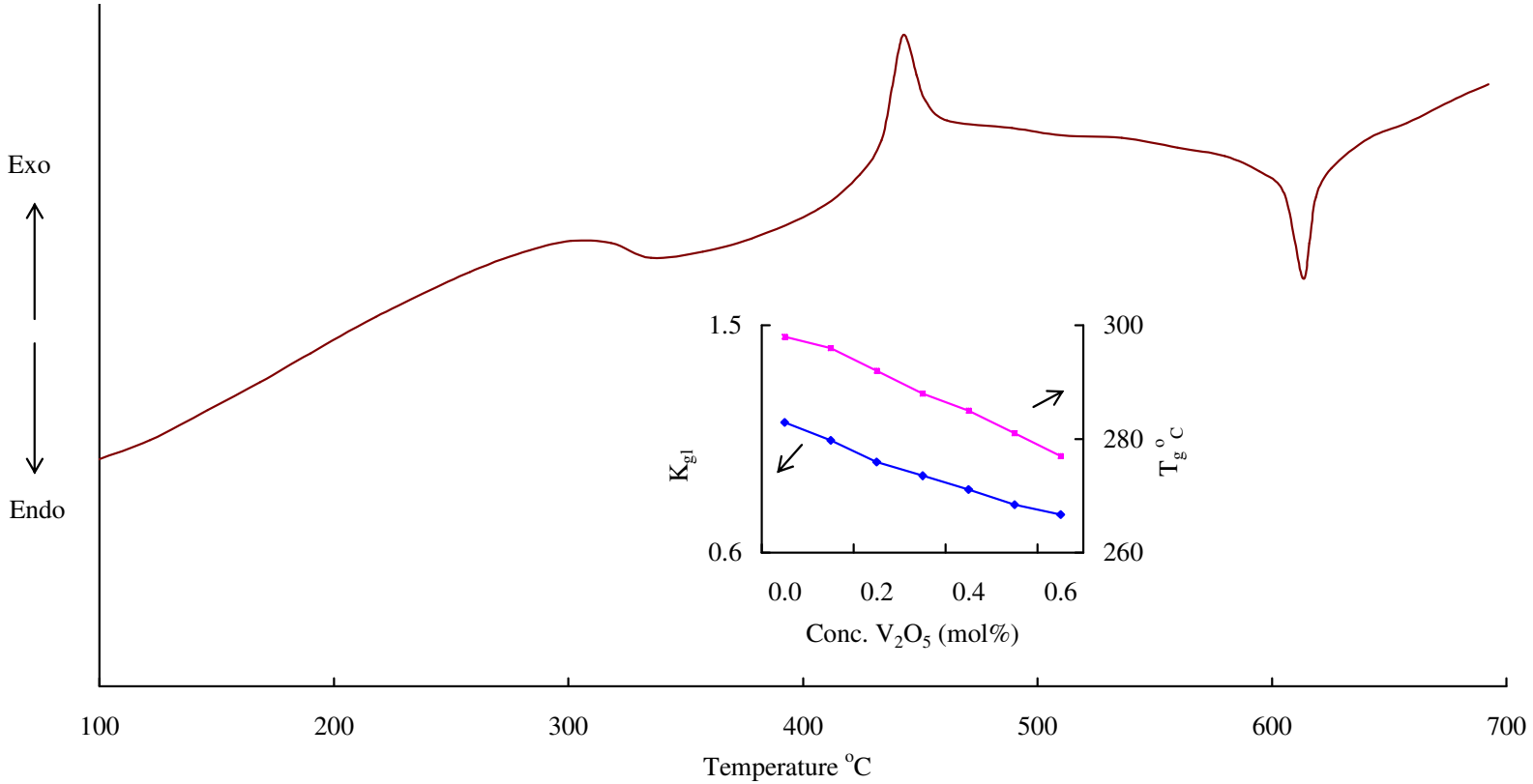

Fig. 3.4 DSC trace of ZnF_2–As_2O_3–TeO_2 glass doped with 0.3 mol% of V_2O_5. Inset shows the variation of T_g and K_{gl} with the concentration of V_2O_5.

Fig. 3.5 represents the optical absorption spectra of ZnF_2–As_2O_3–TeO_2: V_2O_5 glasses recorded at room temperature in the wavelength region 400-1000 nm. The absorption edge observed at 415 nm for glass V_0 (pure glass) is observed to shift towards slightly higher wavelength side with increase in the concentration of V_2O_5. The spectrum of glass V_1 exhibited two broad absorption bands with the meta-centers at 638 and 874 nm (Table 3.2) corresponding to $^2B_2 \rightarrow {}^2B_1$ and $^2B_2 \rightarrow {}^2E$ transitions of VO^{2+} ions [69]; with gradual increase in the concentration of V_2O_5, the half width and peak height of these bands are observed to increase.

Table 3.2. Data on optical absorption spectra of ZnF_2–As_2O_3–TeO_2: V_2O_5 glasses.

Glass	Position of $^2B_2 \rightarrow {}^2B_1$ band (nm)	Position of $^2B_2 \rightarrow {}^2E$ band (nm)	Cut-off wavelength (nm)	Optical band gap E_o (eV)
V_0	-	-	415	2.80
V_1	636	874	461	2.55
V_2	638	875	469	2.50
V_3	640	876	485	2.41
V_4	641	877	486	2.39
V_5	642	879	504	2.24
V_6	643	880	512	2.21

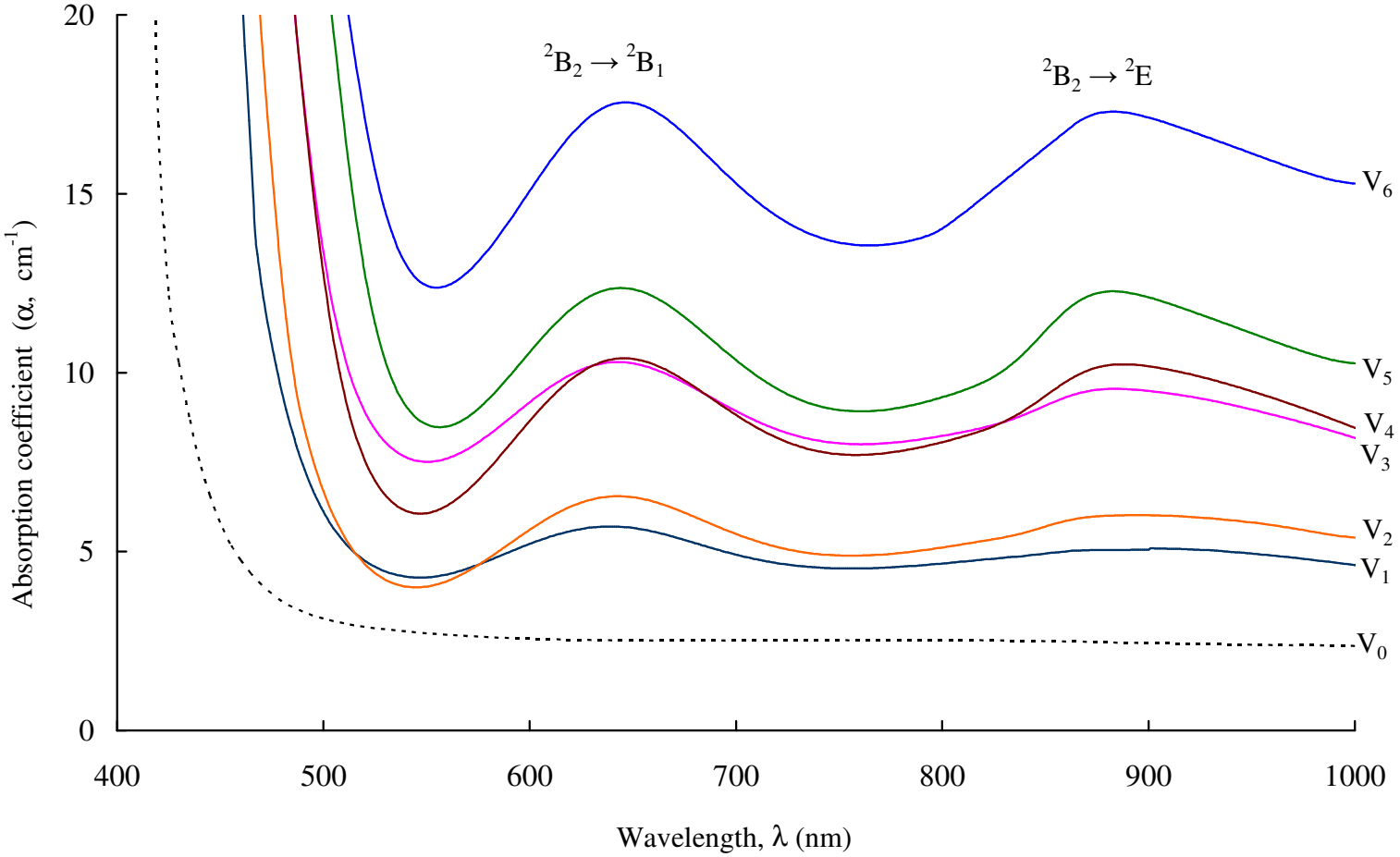

Fig. 3.4 Optical absorption spectra of ZnF_2–As_2O_3–TeO_2: V_2O_5 glasses.

Fig. 3.6 shows the photoluminescence spectra of ZnF_2–As_2O_3–TeO_2: V_2O_5 glasses recorded at room temperature with the excitation wavelength of 640 nm. The spectrum of each glass exhibits a broad emission band in the region 750-850 nm; this band is identified due to $^2E \rightarrow {}^2T_2$ transition of vanadyl ion, the band exhibits a slight asymmetry in the higher wavelength region. With the growing content of V_2O_5 in the glass matrix, the half width of the peak is observed to increase.

The ESR spectra, recorded at room temperature for ZnF_2–As_2O_3–TeO_2: V_2O_5 glasses under investigation are shown in Fig. 3.7; spectra are observed to be complex made up of resolved hyperfine components arising from unpaired $3d^1$ electron of ^{51}V isotope having spin 7/2. As the concentration of V_2O_5 is increased, an increase in the intensity of signal has been observed. The values of $g_{\parallel}$ (1.918) and $g_{\perp}$ (1.979) obtained for the glass V_1 from these spectra, are observed to increase with increase in the concentration of V_2O_5. The pertinent data related to ESR spectra of these glasses are furnished in Tables 3.3 and 3.4.

Table 3.3 ESR parameters of ZnF_2–As_2O_3–TeO_2: V_2O_5 glasses.

Glass	$g_{\parallel}$	$g_{\perp}$	$A_{\parallel}$ x 10^4 (cm^{-1})	$A_{\perp}$ x 10^4 (cm^{-1})
V_1	1.918	1.979	192.1	59.08
V_2	1.919	1.980	190.1	60.03
V_3	1.921	1.982	189.2	60.23
V_4	1.922	1.983	189.0	61.26
V_5	1.923	1.985	186.9	61.27
V_6	1.924	1.986	184.8	62.30

Table 3.4 Covalency parameters of ZnF_2–As_2O_3–TeO_2: V_2O_5 glasses.

Glass	$\Delta g_{\parallel}$	$\Delta g_{\perp}$	$\Delta g_{\perp}/\Delta g_{\parallel}$	α^2	γ^2
V_1	0.084	0.023	0.276	0.665	0.535
V_2	0.083	0.022	0.268	0.655	0.511
V_3	0.081	0.020	0.250	0.637	0.465
V_4	0.080	0.019	0.240	0.628	0.441
V_5	0.079	0.017	0.218	0.619	0.395
V_6	0.078	0.016	0.208	0.611	0.372

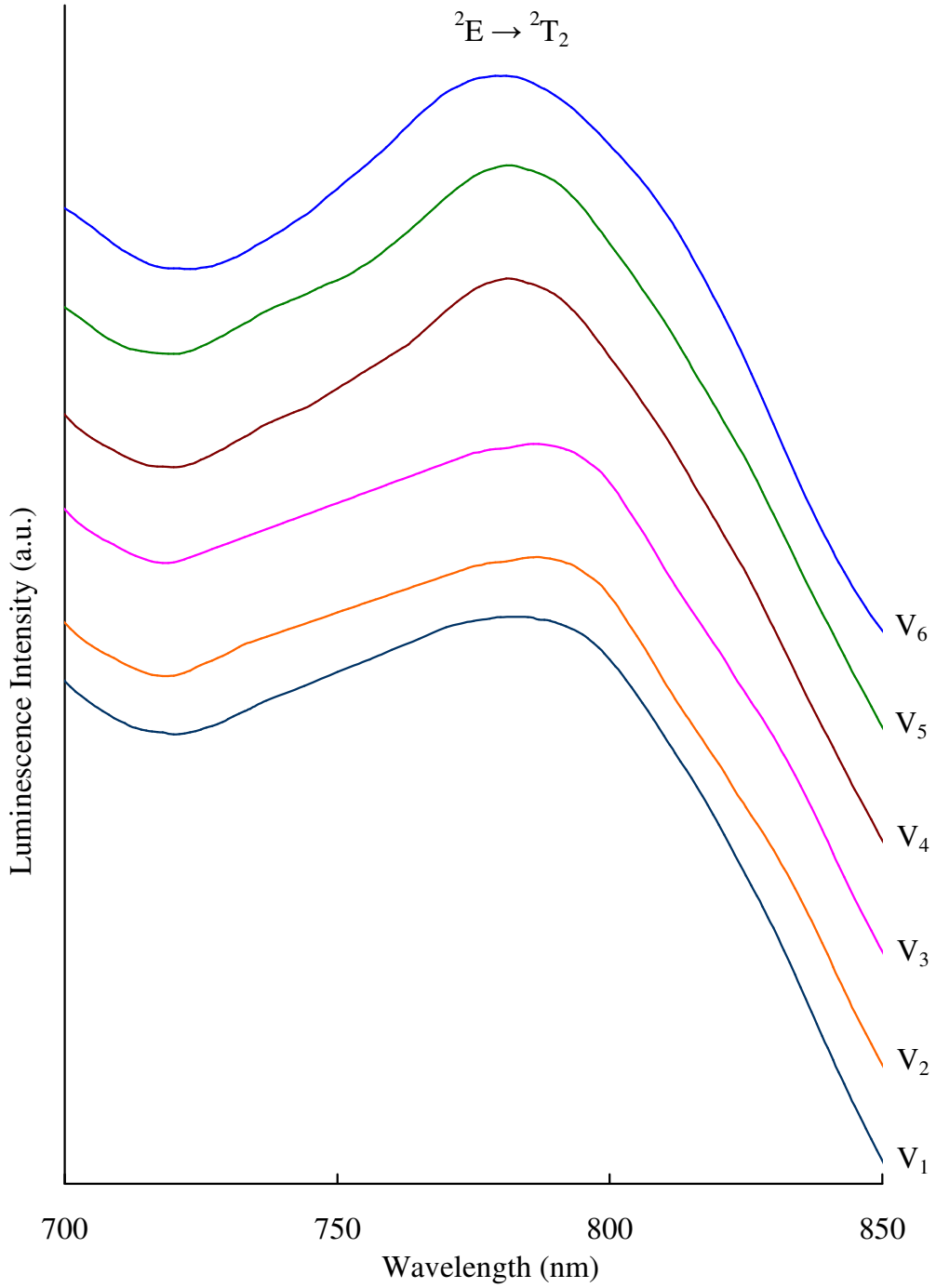

Fig. 3.6 Photoluminescence of ZnF_2–As_2O_3–TeO_2: V_2O_5 glasses recorded at room temperature (λ_{exc}=640nm).

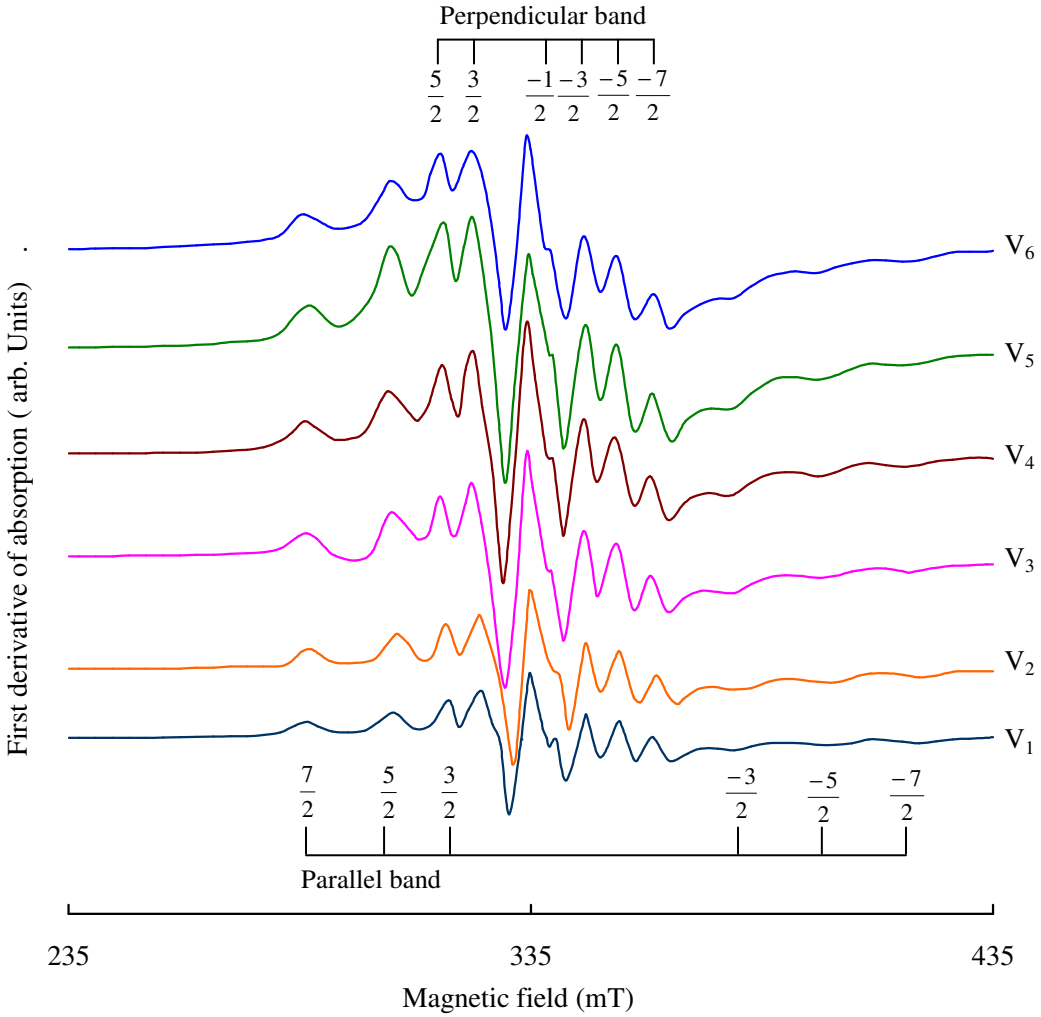

Fig. 3.7 ESR spectra of ZnF_2–As_2O_3–TeO_2: V_2O_5 glasses recorded at room temperature.

Fig. 3.8 shows infrared transmission spectra of ZnF_2–As_2O_3–TeO_2: V_2O_5 glasses. The spectra exhibited different absorption bands due to various structural units of TeO_2 and As_2O_3. IR spectrum of crystalline TeO_2 is expected to exhibit two absorption bands at 772 cm^{-1} [$\nu_1(A_1)$] and at 650 cm^{-1} [$\nu_2(A_2)$] due to ν_s–TeO_{2eq} and ν_s–TeO_{2ax} vibrations with C_{2v} symmetry, respectively [70]. Similarly four prominent bands are expected in the IR spectrum of crystalline As_2O_3 due to ν_1 (1050 cm^{-1}), ν_2 (625 cm^{-1}), ν_3 (812 cm^{-1}) and ν_4 (495 cm^{-1}) vibrations of AsO_3 structural units [71]. In the spectrum of glass V_0 (Fig. 3.8) the vibrational frequency of ν_s–TeO_{2ax} (axial band) is located at 643 cm^{-1} whereas the ν_s–TeO_{2eq} is observed to be missing; the ν_1 and ν_2-bands of AsO_3 structural groups are located at 1007 and 620 cm^{-1} respectively; the ν_4-band of these structural groups is also positioned at about 431 cm^{-1}. With the introduction of V_2O_5, the ν_s–TeO_{2ax} and ν_2 of AsO_3 bands are shifted gradually towards considerably higher frequencies (Table 3.5). Additionally, a band due to V–O–V vibrations is also observed at about 790 cm^{-1} in the spectrum of glass V_1. The vibrations of isolated V=O groups in VO_5 trigonal bipyramids is also expected to exhibit a band at about 1000 cm^{-1} in V_2O_5 doped glasses [72]; this band seems to be merged with ν_1 vibrations of AsO_3 structural units in the spectrum of glass V_1. As a result we may assume the observed band at about 1000 cm^{-1} in the spectrum of glass V_1 is due to V–O–As common vibrations. With the gradual increase in the concentration of V_2O_5, these two bands have

been separated and are observed to grow separately in proportional to the concentration of V_2O_5 in the glass matrix. A new band identified due to bending vibrations of V–O–V chains at about 600 cm^{-1} is also detected in the spectra of V_2O_5 doped glasses. The summary of various band positions of the IR spectra of these glasses is furnished in Table 3.5.

Table 3.5 Summary of the data on IR spectra of ZnF_2–As_2O_3–TeO_2:V_2O_5 glasses. The band positions given are in cm^{-1}.

Assignment	Glass V_0	Glass V_1	Glass V_2	Glass V_3	Glass V_4	Glass V_5	Glass V_6
ν_1 As_2O_3	1007	1017	1025	1032	1041	1050	1060
V=O	-	-	-	977	980	985	998
V–O–V chains	-	787	789	796	808	813	817
ν^s_{ax} TeO_2	643	645	646	648	650	651	655
ν_2 As_2O_3	620	623	626	627	629	630	632
V–O–V bending	-	594	594	596	597	599	600
ν_4 As_2O_3	431	433	436	438	439	440	442

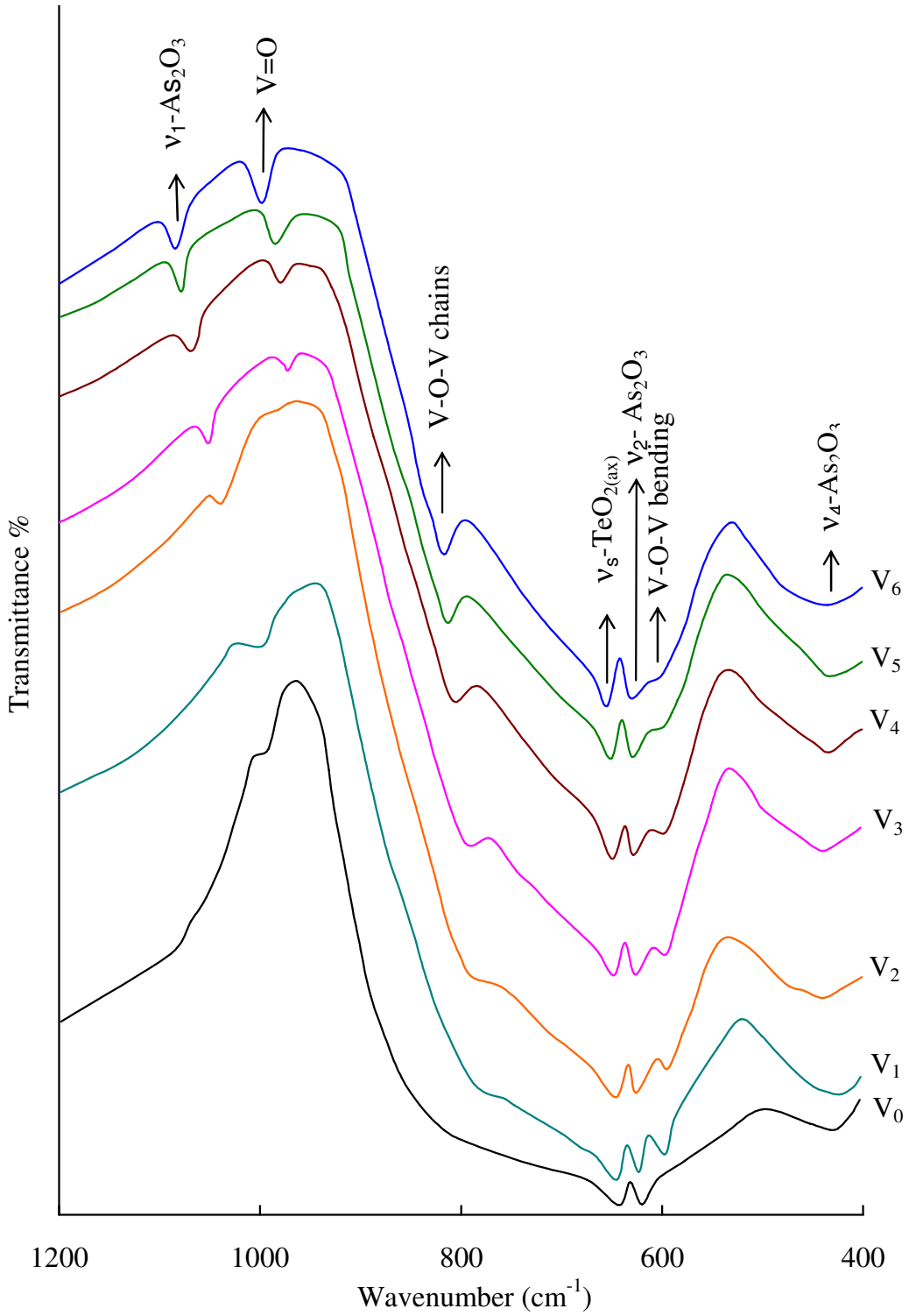

Fig. 3.8 Infrared transmission spectra of ZnF_2–As_2O_3–TeO_2:V_2O_5 glasses recorded at room temperature.

The dielectric constant ε' and loss tanδ at room temperature (30 ^{o}C) of pure ZnF_2–As_2O_3–TeO_2 glasses at 100 kHz are measured to be 18.5 and 0.008 respectively. The values of ε' and tanδ of all the samples are found to increase considerably with decrease in frequency. Fig. 3.9 represents the variation of dielectric constant and loss with frequency of ZnF_2–As_2O_3–TeO_2 glasses doped with different concentrations of V_2O_5, measured at room temperature; the parameters ε' and tanδ are observed to increase with the concentration of V_2O_5. Inset of the same figure shows the variation of dielectric constant and loss with the concentration of V_2O_5 measured at 10 kHz. The parameters, ε' and tanδ are observed to increase with the concentration of V_2O_5.

The temperature dependence of ε' at different frequencies for one of the glass viz., V_6 and that of the glasses doped with different concentrations of V_2O_5 at 1 kHz are shown in Fig. 3.10. The value of ε' is found to exhibit a considerable increase at higher temperatures especially at lower frequencies; the rate of increase of ε' with temperature is found to be the highest for the glass containing the highest concentration of V_2O_5.

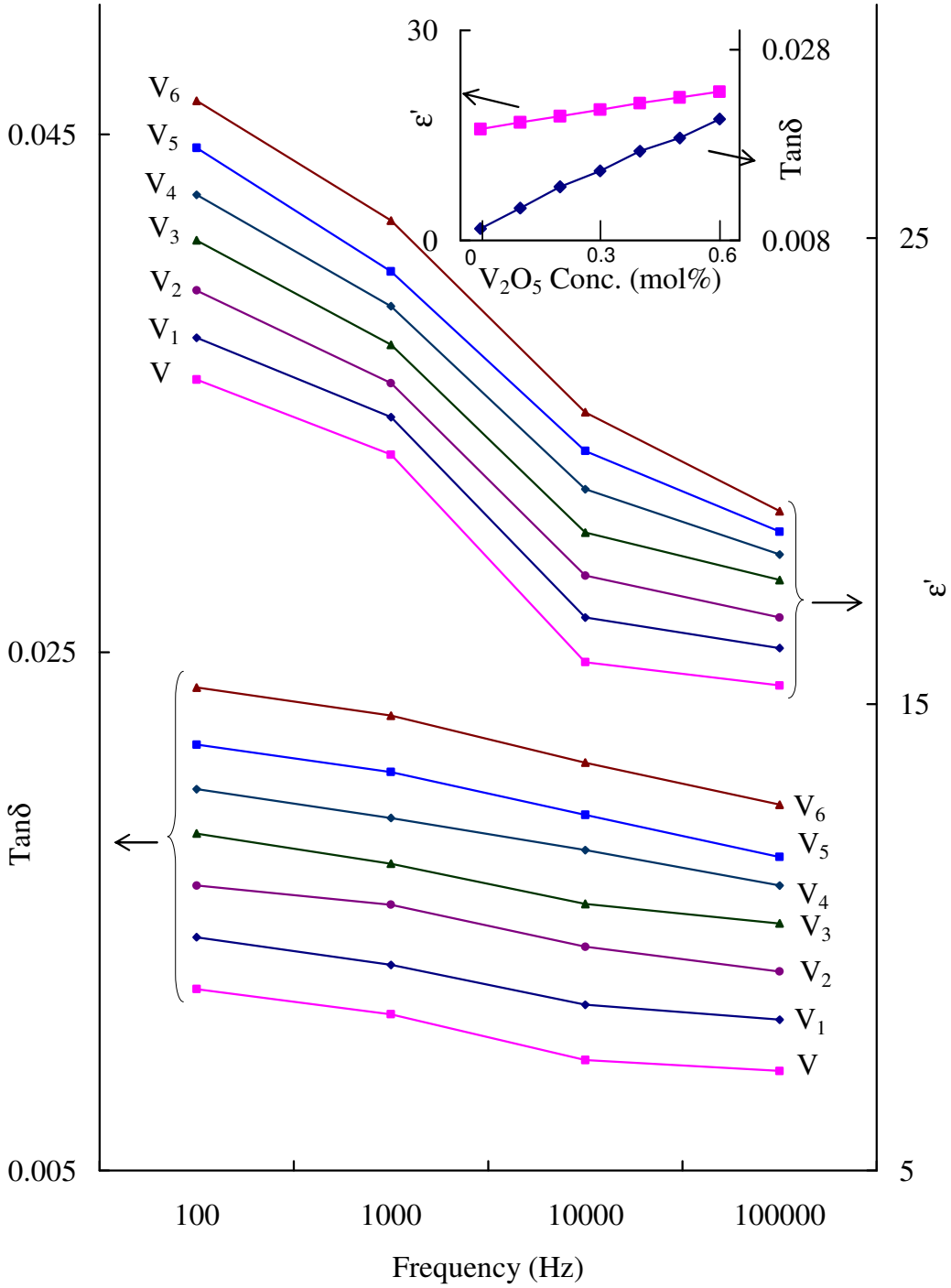

Fig. 3.9 Variation of dielectric constant and loss with the frequency of ZnF_2–As_2O_3–TeO_2 glasses containing different concentrations of V_2O_5 measured at room temperature. Inset gives the variation of ε' and tanδ with the concentration of V_2O_5 measured at 10 kHz.

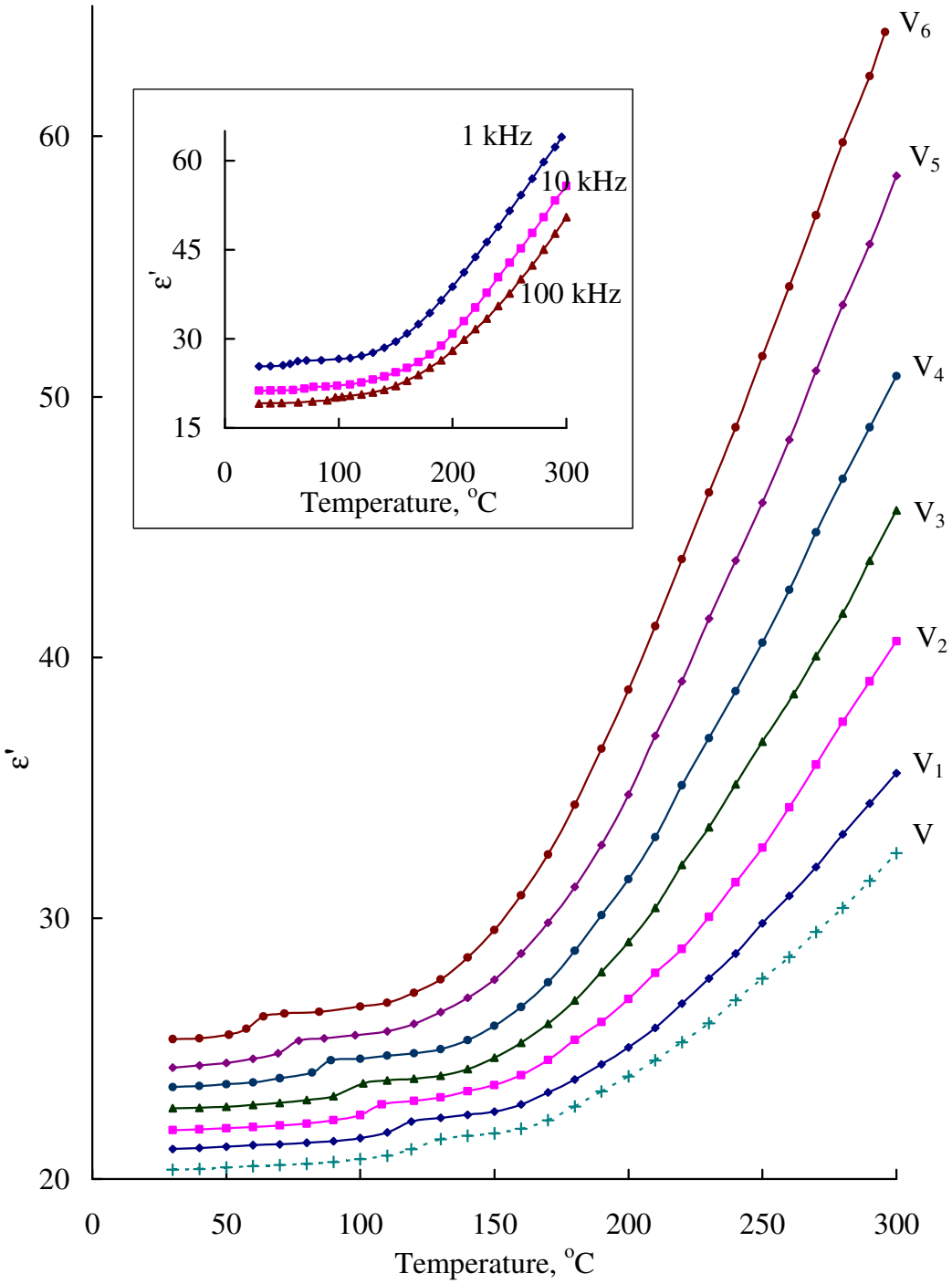

Fig. 3.10 A comparison plot of variation of dielectric constant with temperature at 1 kHz for ZnF_2–As_2O_3–TeO_2: V_2O_5 glasses. Inset shows variation of dielectric constant with temperature at different frequencies for glass containing 0.6 mol% of V_2O_5.

The temperature dependence of tan δ of glass V_4 (glass containing 0.4 mol % of V_2O_5) at different frequencies (inset (a)) and a comparison plot of variation of tanδ with temperature, measured at a frequency of 100 kHz are presented in Fig. 3.11. The pertinent data related to dielectric loss of these glasses is presented in Table 3.6.

Table 3.6 Data on dielectric loss of ZnF_2–As_2O_3–TeO_2: V_2O_5 glasses.

Glass	$(Tan\delta_{max})_{avg}$	Temperature region of relaxation (^oC)	Activation energy for dipoles (eV)
V_0	0.026	130–147	2.52
V_1	0.028	120–140	2.44
V_2	0.030	108–130	2.30
V_3	0.031	103–126	2.18
V_4	0.033	94–118	1.96
V_5	0.036	83–108	1.43
V_6	0.039	70–97	1.27

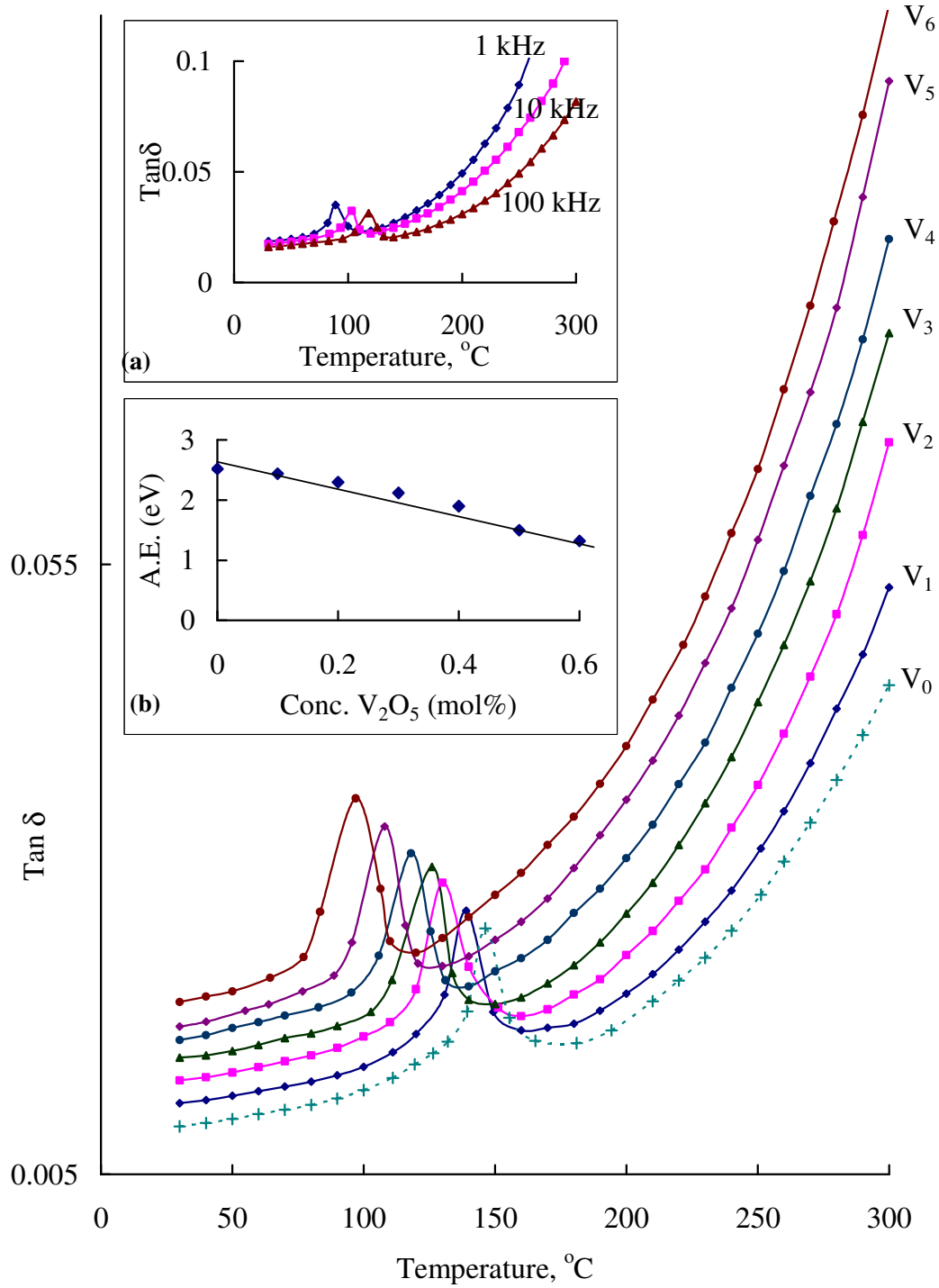

Fig. 3.11 A comparison plot of variation of dielectric loss with temperature for ZnF_2–As_2O_3–TeO_2: V_2O_5 glasses measured at 100 kHz. Inset (a) shows the variation of dielectric loss with temperature for the glass V_4 at different frequencies. Inset (b) shows variation of activation energy for dipoles with the concentration of V_2O_5.

The ac conductivity σ_{ac} is calculated at different temperatures using the equation:

$$\sigma_{ac} = \omega \varepsilon' \varepsilon_o \tan\delta, \qquad (3.1)$$

(where ε_o is the vacuum dielectric constant) for different frequencies and the plot of log σ_{ac} against 1/T for all the glasses at 1 kHz in Fig. 3.12; the conductivity is found to increase considerably with increase in the concentration of V_2O_5 at any given frequency and temperature (inset (a) of Fig. 3.12). From these plots, the activation energy for the conduction in the high temperature region over which a near linear dependence of log σ_{ac} with 1/T could be observed is evaluated and presented in Table 3.7; the activation energy is found to decrease with increase of V_2O_5 content in the glass matrix.

Table 3.7 Data on ac conductivity of ZnF_2–As_2O_3–TeO_2: V_2O_5 glasses.

Glass	$N(E_F)$ in (10^{20}, eV^{-1}/cm^3)	A.E for conduction (eV)
V_0	2.35	0.72
V_1	2.55	0.59
V_2	2.81	0.54
V_3	3.02	0.50
V_4	3.22	0.43
V_5	3.42	0.37
V_6	3.68	0.35

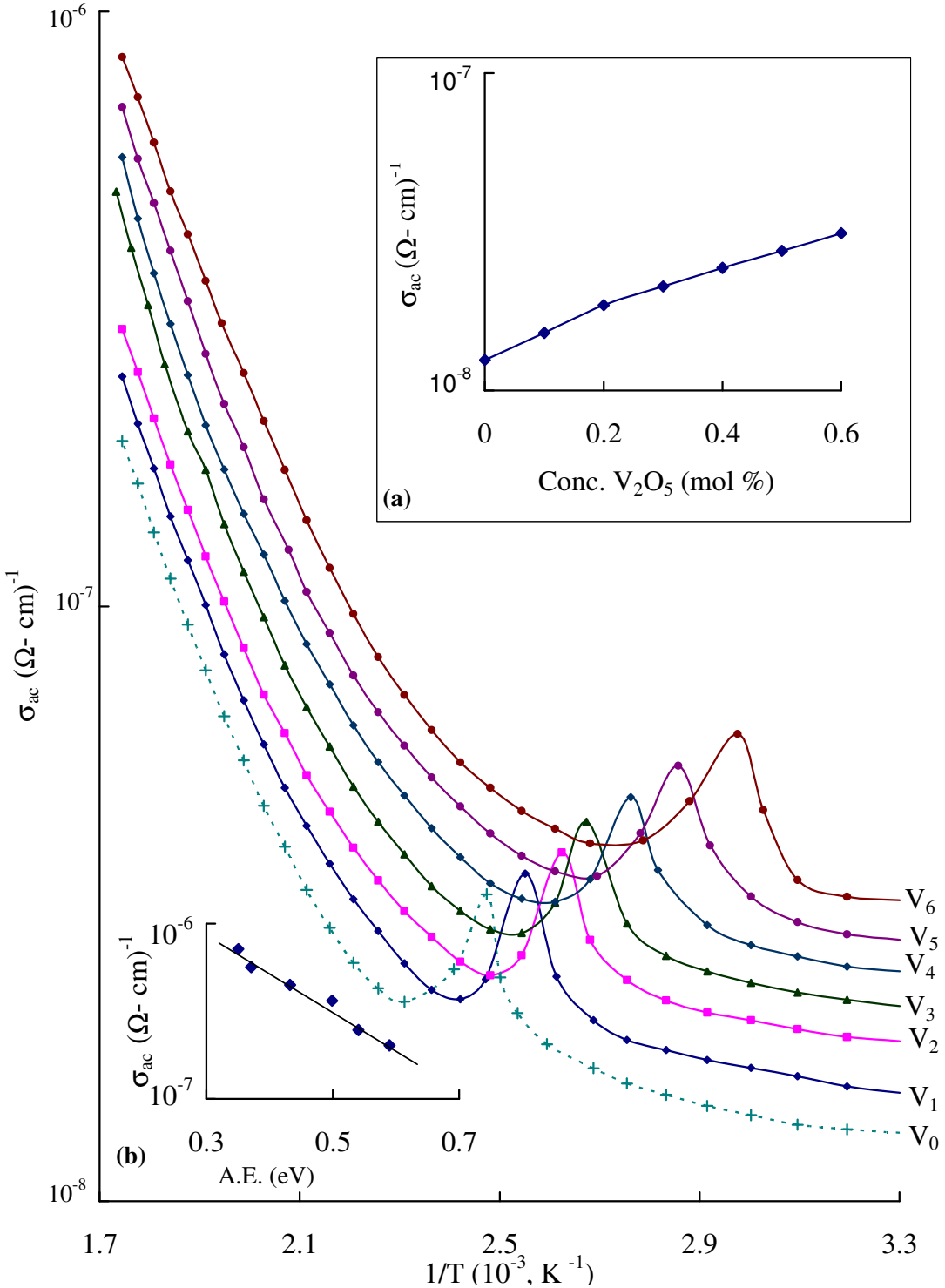

Fig. 3.12 A comparison plot of variation of ac conductivity with 1/T at 1 kHz for ZnF_2–As_2O_3–TeO_2: V_2O_5 glasses. Inset (a) gives the variation of σac with the concentration of V_2O_5 and (b) gives the variation of σac with the activation energy for conduction.

3.4. Discussion

TeO_2 is an intermediate glass forming oxide; it is an incipient glass network former and as such does not readily form glass since the octahedral Te–O polyhedron is highly rigid (when compared with other glass forming oxides like GeO_2 etc.) to get required distortion of Te–O bonds, necessary for forming a stable network. Earlier neutron scattering experiments [73] and Raman spectral studies [74] on TeO_2 glasses containing different modifiers have revealed that the basic building block of TeO_2 glass structure is a trigonal bipyramid commonly called TeO_4E, where one of the three equatorial directions is occupied by the $5s^2$ electronic pair (E) of the tellurium atom with two equatorial bonds of lengths 1.91 °A and two axial bonds of lengths 2.08 °A [73, 74]. The environment of these Te atoms is completed by two other longer interactions of lengths 2.9 °A and the three dimensional close packing is constituted from vertices sharing TeO_4 groups (Te_{eq}–O_{ax}–Te) reinforced by weaker Te-O interactions of lengths 2.9 °A [70, 75]. In general ZnF_2 acts as modifier, fluorine ions break the Te–O bonds while Zn^{2+} ions may occupy interstitial positions or form Zn–O–Te linkages because of the close ionic radii of Te^{4+} (0.7 °A) and Zn^{2+} (0.74 °A) ions.

As_2O_3 is a strong network former with corner sharing AsO_3 pyramidal units; normal bond lengths of As–O lie in between 1.72 and 1.812 °A and O–As–O and As–O–As bond angles lie in the range 90–103^o and 123–135^o,

respectively [76]. Vanadium ions seem to exist mainly in V^{4+} and V^{5+} states in the present of ZnF_2–As_2O_3–TeO_2: V_2O_5 glass network. During the melting of the glasses at higher temperatures, there is every possibility for the following redox equilibria to take place:

$$2V^{5+} + O^{2-} \rightarrow 2V^{4+} + (1/2)O_2\uparrow;$$

$$As_2O_3 + V_2O_5 \rightarrow As_2O_5 + V_2O_3$$

The later equation suggests that a small number of V^{5+} ions may also reduce to V^{3+} state [77]. The V^{5+} ions take part network-forming positions with VO_5 structural units whereas the V^{4+} ions may distort the glass network. As mentioned earlier, both TeO_2 and As_2O_3 participate in the glass network with TeO_4 and AsO_3 pyramids. On the other hand, $As^{(V)}{}_2O_5$ may participate in the glass network with $As^{V}O_4$ units and play a similar structural role to BO_4 units in the borate network and form the linkages of the type As–O–Te. As a modifiers, V^{4+} ions enters the glass network by breaking up Zn–O–Te, As–O–Te bonds, and TeO_4 bonds and may introduce: (i) the stable $Te–O^-$ and (ii) unstable $Te–O^-$ bonds which will later be modified to $Te–O^-$ (or simply TeO_{3+1}) owing to the contraction of one $Te–O^-$ and the elongation of another $Te\text{-}O^-$ bond. With increasing V_2O_5 content (up to 0.6 mol%), cleavage of continuous network leads to an increase in the fraction of TeO_{3+1} polyhedra. Further, the elongation of Te–O bond of TeO_{3+1} and its cleavage finally lead to the formation of trigonal prismatic TeO_3 units (Fig. 3.13). Thus in addition to

AsO_3, Te–O–Te, Zn–O–Te linkages, the structure of the present glass network consists of TeO_4, TeO_{3+1} and TeO_3, free Zn^{2+} ions, free F^- ions VO^{2+} complexes and non bridging oxygens. Such bonding defects may increase with increase in the concentration of V_2O_5.

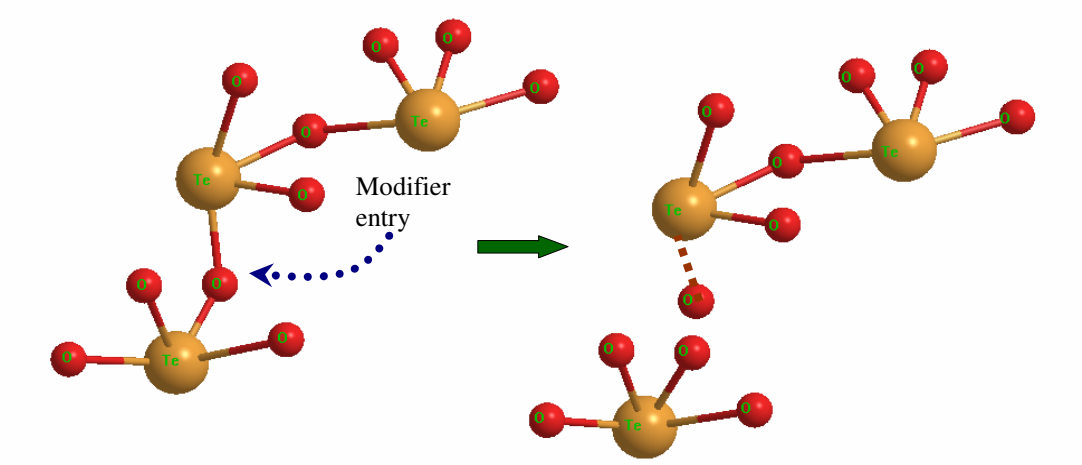

Fig. 3.13 A mechanism for structural change in TeO_2 glass network from TeO_4 (tbp) to TeO_{3+1} polyhedra induced by modifier.

The DSC studies have indicated that the values of the glass transition temperature Tg and glass forming ability parameter K_{gl}, to decrease with increase in the concentration of V_2O_5 in the glass matrix. This observation pointsout that there is an increasing concentration of vanadyl ions that act as modifier with increase in the content of V_2O_5 in the glass matrix.

The electronic configuration of V^{4+} ion is $3d^1$ and its ground state is 2D. The presence of pure octahedral crystal field, the 2D state splits into $^2T_2$ and ^2E, while an octahedral field with tetragonal distortion the $^2T_2$ state further splits into three $^2B_2$ (viz. $|xy$, $|yz$ and $|zx$) states and ^2E excited state splits into $A_1 \left|3z^2 - r^2\right\rangle$ and $B_1 \left|x^2 - y^2\right\rangle$ (ground state). Thus for the vanadyl ions we can

expect three absorption bands (on the basis of energy level scheme) for molecular orbitals of VO^{2+} ion in a ligand field of C_{4v} symmetry provided by Ballhausen and Gray [69] corresponding to the transitions $^2B_2 \rightarrow {}^2B_1$, $^2B_2 \rightarrow {}^2E$ and $^2B_2 \rightarrow {}^2A_1$. However, in the spectra of the present glasses, only the first two bands have been observed. The intensity and the half width of these bands have been observed to be maximal in the spectrum of glass V_6; this observation indicates the presence of the largest concentration of VO^{2+} (vanadyl) ions in this glass. These VO^{2+} ions are expected to participate in the depolymerisation of the glass network, create more bonding defects and non-bridging oxygens (NBOs) as mentioned earlier. This is also supported by the fact that the symmetrical vibrational frequencies of ν^s_{ax}–TeO_2 bonds of TeO_4 groups in the IR spectra are shifted towards higher frequencies with decreasing intensity as the concentration of V_2O_5 is increased.

From the observed absorption edges, we have evaluated the optical band gaps (E_o) of these glasses by drawing Urbach plot between $(\alpha\ \hbar\omega)^{1/2}$ and $\hbar\omega$ as per the equation:

$$\alpha(\omega)\hbar\omega = C(\hbar\omega - E_o)^2 \qquad (3.2)$$

Fig. 3.14 represents the Urbach plots of all these glasses in which a considerable part of each curve is observed to be linear. The values of optical band gap (E_o) obtained from the extrapolation of these curves are presented in Table 3.2; the value of E_o is found to be the lowest for glass V_6.

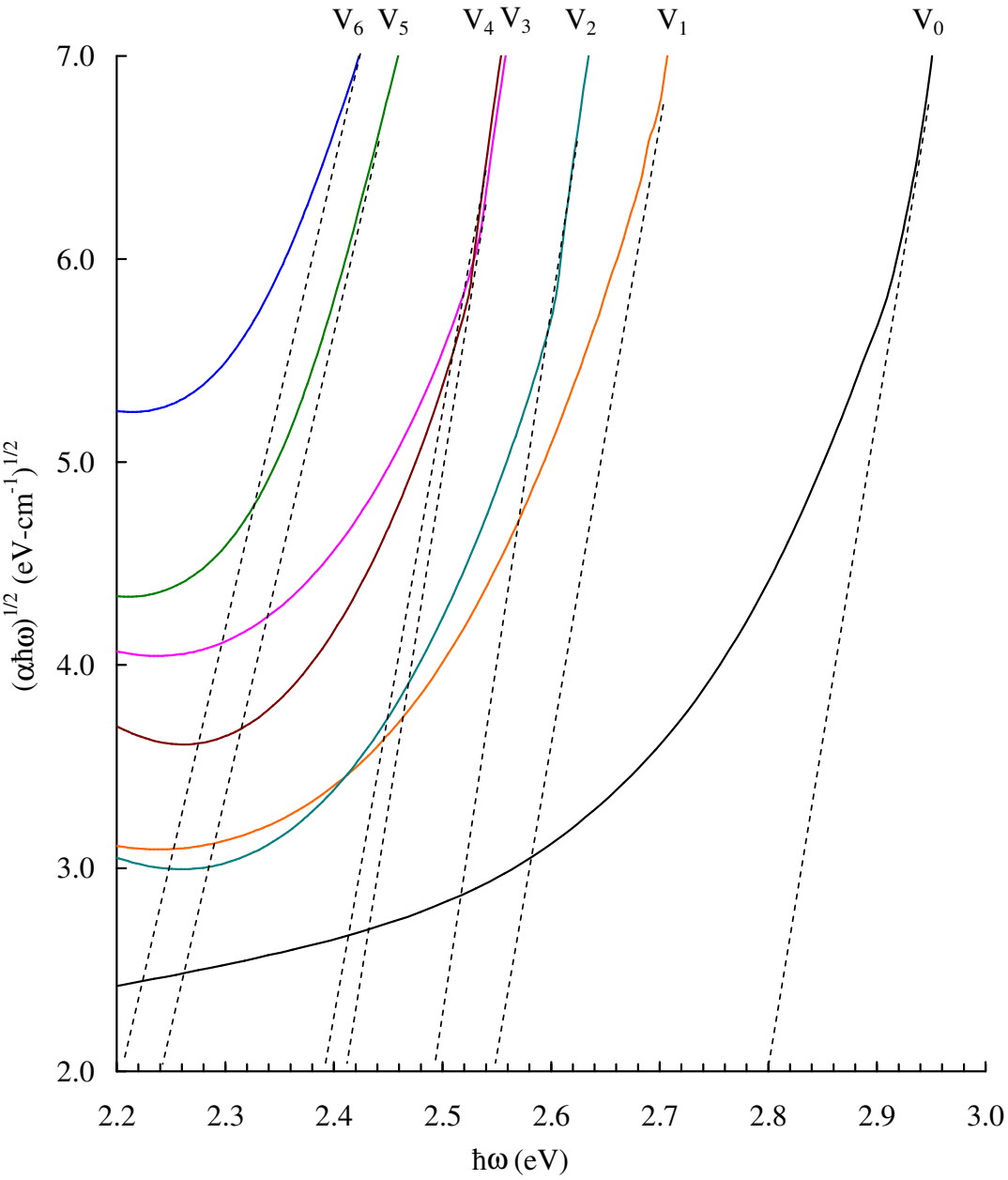

Fig. 3.14 Urbach plots to evaluate optical band gaps for ZnF_2–As_2O_3–TeO_2: V_2O_5 glasses.

The decrease in the optical band gap with the increase in the concentration of the dopant up to 0.6 mol% can be understood as follows: the gradual increase in the concentration of vanadyl ions in the glass network, causes a creation of large number of donor centers; subsequently, the excited states of localized electrons originally trapped on VO^{2+} sites begin to overlap with the empty 3d states on the neighboring V^{5+} sites. As a result, the impurity band becomes more extended into the main band gap. This development shifts the absorption edge to low energy side (Fig. 3.6, Table 3.2) resulting a significant shrinkage in the band gap.

The ESR spectra are in general described by the spin Hamiltonian of axial symmetry:

$$\mathrm{H} = g_{\parallel}\beta H_z S_z + g_{\perp}\beta\left(H_x S_x + H_y S_y\right) + A_{\parallel} S_z I_z + A_{\perp}\left(S_x I_x + S_y I_y\right) \quad (3.3)$$

Where β is the Bohr magneton, $g_{\parallel}$ and $g_{\perp}$ are the parallel and perpendicular components of g-tensor and $A_{\parallel}$ and $A_{\perp}$ are parallel and perpendicular components of hyperfine tensor.

The variation of ESR line width and the resolution with the concentration of V_2O_5 is obviously due to the variation in the concentration of V^{4+} ions and also due to structural and microstructural modifications, that can produce fluctuations of the degree of distortion or even of the coordination geometry of V^{4+} sites. The observed broadening of ESR signal with the concentration of V_2O_5 indicates the growing presence of V^{4+} ions and may also

be due to exchange coupling between V^{3+} ions (if any) and V^{4+} ions [78]. The spectra consists of the well-resolved hyperfine structure with eight components of the electron-nuclear interactions with divergence of magnetic fields given by

$$H_{\parallel}(m_I) = H_{\parallel}(0) - A_{\parallel} m_I - \frac{A_{\perp}^{\,2}}{2H_{\parallel}(0)}\left(\tfrac{63}{4} - m_I^{\,2}\right) \tag{3.4}$$

$$H_{\perp}(m_I) = H_{\perp}(0) - A_{\perp} m_I - \frac{\left(A_{\parallel}^{\,2} + A_{\perp}^{\,2}\right)}{4H_{\perp}(0)}\left(\tfrac{63}{4} - m_I^{\,2}\right) \tag{3.5}$$

Here m_I is the nuclear magnetic quantum number taking the values $\pm 7/2, \pm 5/2, \pm 3/2, \pm 1/2$; $H_{\parallel,\perp} = h\nu / g_{\parallel,\perp}\beta$, ν is the frequency of spectrometer The values of g-tensor and A-tensor obtained for these spectra are presented in Tables 3.3.

The ESR and optical absorption spectral data can be correlated to understand the environment of vanadium ions in ZnF_2–As_2O_3–TeO_2 glass network are described below. The g parameters are given by [79]:

$$g_{\parallel} = g_e\left[1 - \frac{4\lambda\alpha^2}{E(^2B_1)}\right] \tag{3.6}$$

$$g_{\perp} = g_e\left[1 - \frac{\lambda\gamma^2}{E(^2E)}\right] \tag{3.7}$$

where λ is the spin–orbit coupling coefficient (249 cm^{-1} for V^{4+} ion) and the bonding coefficients α^2, γ^2 characterize respectively, the in –plane σ bonding and out of –plane π bonding of the V^{4+} ions.

The bonding scheme between vanadium and oxygen ions can be further illustrated as follows: a very strong σ bond will be formed between the ($2p_z$+2s) hybrid of the oxygen and the $(3d_{z^2} + 4s)$hybrid of the vanadium ion. Furthermore, the $2p_x$ and $2p_y$ orbitals on the oxygen do make a strong π bond with the $3d_{xz}$, $3d_{yz}$ orbitals on the metal ion, as a result VO^{2+} becomes a highly stable complex. The $(3d_{z^2} - 4s)$ hybrid, together with the orbitals $(3d_{x^2-y^2})$ and $4p_x$, $4p_y$ and $4p_z$ are then just capable of five σ bonds directed in a tetragonal pyramid with the V^{4+} ion located at its base.

From eqns (3.6) and (3.7),

$$\frac{\Delta g_{\perp}}{\Delta g_{\parallel}} = \frac{4E(^2B_1)\gamma^2}{E(^2E)\alpha^2} \quad \propto \quad \frac{\gamma^2}{\alpha^2} \tag{3.8}$$

The values of $\Delta g_{\perp}/\Delta g_{\parallel}$ obtained for the glasses containing different concentrations of V_2O_5 are presented in Table 3.4; the ratio is observed to decrease gradually with increase in the concentration of V_2O_5. As we see in the Table 3.4, the γ^2 is always less than α^2; in other words the covalency factor ($1-\gamma^2$) is always greater than ($1-\alpha^2$) or the ratio of $(1-\gamma^2)/(1-\alpha^2)$ goes on increasing with increase in the concentration of V_2O_5. Such result indicates a progressive weakening of the bonding between V^{4+} ion and equatorial oxygen as the concentration of V_2O_5 is increased; this leads to an increase in the degree of disorder of the octahedral and in the glass network as a whole.

Excitation of ZnF_2–As_2O_3–TeO_2: V_2O_5 glass samples with the wavelength corresponding to $^2B_2 \rightarrow {}^2B_1$, resulted a broad emission band as shown in Fig. 3.8. Since the wavelength of this band is close to the maximum of the band $^2B_2 \rightarrow {}^2E$, we attribute this band as the $^2E \rightarrow {}^2T_2$ transition of V^{4+} ions; the emission band is relatively broad and structureless. With increase in the concentration of V_2O_5, the intensity of the peak is observed to increase with a red shift. The shift of this PL peak, the shape and the structured nature of the PL emission band are a signature of shallow levels with an electron–phonon coupling. The distortion of the luminescence band in the lower energy side is probably due to the reabsorption by V^{3+} ions if any in the glass network [80].

The dielectric constant of a material is due to electronic, ionic, dipolar and space charge polarizations. Out of these, the space charge contribution depends on the purity and the perfection of the glasses. Its influence is in general negligible at very low temperatures and noticeable in the low frequency region. The dipolar effects can some times be seen in the glasses even up to 10^6 Hz. Recollecting the data the slight increase in the dielectric constant and loss at room temperature, particularly at low frequencies for ZnF_2–As_2O_3–TeO_2: V_2O_5 glasses may be ascribed to the defects produced in the glass network which contribute to the space charge polarization. With the gradual increase of the dopant V_2O_5 from 0 to 0.6 mol%, the values ε', tan δ and σ_{ac} are found to increase at any frequency and temperature and activation

energy for ac conduction is observed to decrease; this is an indication of an increase in the space charge polarization. Such increase is probably due to the presence of higher concentration of V^{4+} ions in the glass network that act as modifiers and generate bonding defects in the glass network. The defects thus produced create easy path ways for the migration of charges that would build up space charge polarization and facilitate to an increase in the dielectric parameters as observed [81–83].

The variation of dielectric loss with the temperature has exhibited distinct maxima; with increasing frequency the temperature maximum shifts towards higher temperature and with increasing temperature the frequency maximum shifts towards higher frequency, indicating the dielectric relaxation character of dielectric losses of these glasses. Further, the observations on dielectric loss variation with temperature for different concentrations of V_2O_5 indicate an increase in the broadness and $(\tan\delta)_{max}$ of relaxation curves with a shift of $\tan\delta_{max}$ towards lower temperature with increase in the concentration of V_2O_5.

The effective activation energy $W_{d,}$ for the dipoles is evaluated for all the glasses using the relation

$$f = f_o e^{-W_d / kT} \tag{3.9}$$

and its variation with the concentration of V_2O_5 is shown as inset (b) of Fig. 3.11. The activation energy is found to decrease with the concentration of V_2O_5 in accordance with the energy gap behavior.

The way the dielectric constant and the loss vary with the frequency and temperature suggests that these glasses exhibit dielectric relaxation effects. Conventionally, the dielectric relaxation effects are described with the variable frequency at a fixed temperature. However, similar information can also be obtained by analyzing these results at a fixed frequency at variable temperature as suggested by Bottcher and Bordewijk [84].

Substituting the eqn. (3.9) in standard Debye relations for dielectric relaxation, viz.,

$$\varepsilon'(\omega) = \varepsilon_\infty + \frac{\varepsilon_s - \varepsilon_\infty}{1+\omega^2\tau^2} \tag{3.10}$$

$$\varepsilon''(\omega) = \frac{(\varepsilon_s - \varepsilon_\infty)\omega\tau}{1+\omega^2\tau^2} \tag{3.11}$$

one can obtain

$$\varepsilon'(\omega,T) = \varepsilon_\infty + \tfrac{1}{2}(\varepsilon_s - \varepsilon_\infty)\left[1 - tgh(E_a/kT + \ln\omega A)\right] \tag{3.12}$$

$$\varepsilon''(\omega,T) = \frac{\tfrac{1}{2}(\varepsilon_s - \varepsilon_\infty)}{\cosh(E_a/kT + \ln\omega A)} \tag{3.13}$$

In eqns. (3.12) and (3.13), ε_∞ is temperature independent whereas ε_s is largely dependent on temperature. Keeping in mind, the variation of hyperbolic

trigonometric functions in eqns. (3.12) and (3.13) with temperature is very minute, these eqns. can be rewritten as

$$\varepsilon'(\omega,T) = \varepsilon_\infty + \tfrac{1}{2}(\varepsilon_s - \varepsilon_\infty)\left[1 - tgh\{E_a(1/T - 1/T_m(\omega))/k\}\right] \quad (3.14)$$

$$\text{and } \varepsilon''(\omega,T) = \frac{\tfrac{1}{2}(\varepsilon_s - \varepsilon_\infty)}{\cosh\left[E_a(1/T - 1/T_m(\omega))/k\right]} \quad (3.15)$$

In these eqns. $T_m(\omega)$ is the temperature at where ε' exhibits maximum value. Thus, as per the eqns. (3.14) and (3.15), the plots of ε'(ω, T) and ε" (ω, T) against 1/T should be centro symmetric and symmetric curves respectively in the dielectric relaxation region.

As an example for one of the glass samples (viz., V_6) under investigation, the variation of ε'(ω, T) and ε" (ω, T) with 1/T are shown in Fig. 3.15. The shape of these curves is well in accordance with the eqns. (3.14) and (3.15) and clearly confirms the relaxation character of dielectric properties of these glasses.

Among the three constituents viz., ZnF_2, As_2O_3 and TeO_2 of these glasses, the bonds of tellurium with oxygen are known to be polar in nature [85] and hence it is reasonable to attribute the observed dipolar effects in these glasses to the TeO_4 structural units [86, 87]. Further, the way the dielectric loss varies with the temperature for all the samples indicate that there is a spreading of relaxation times.

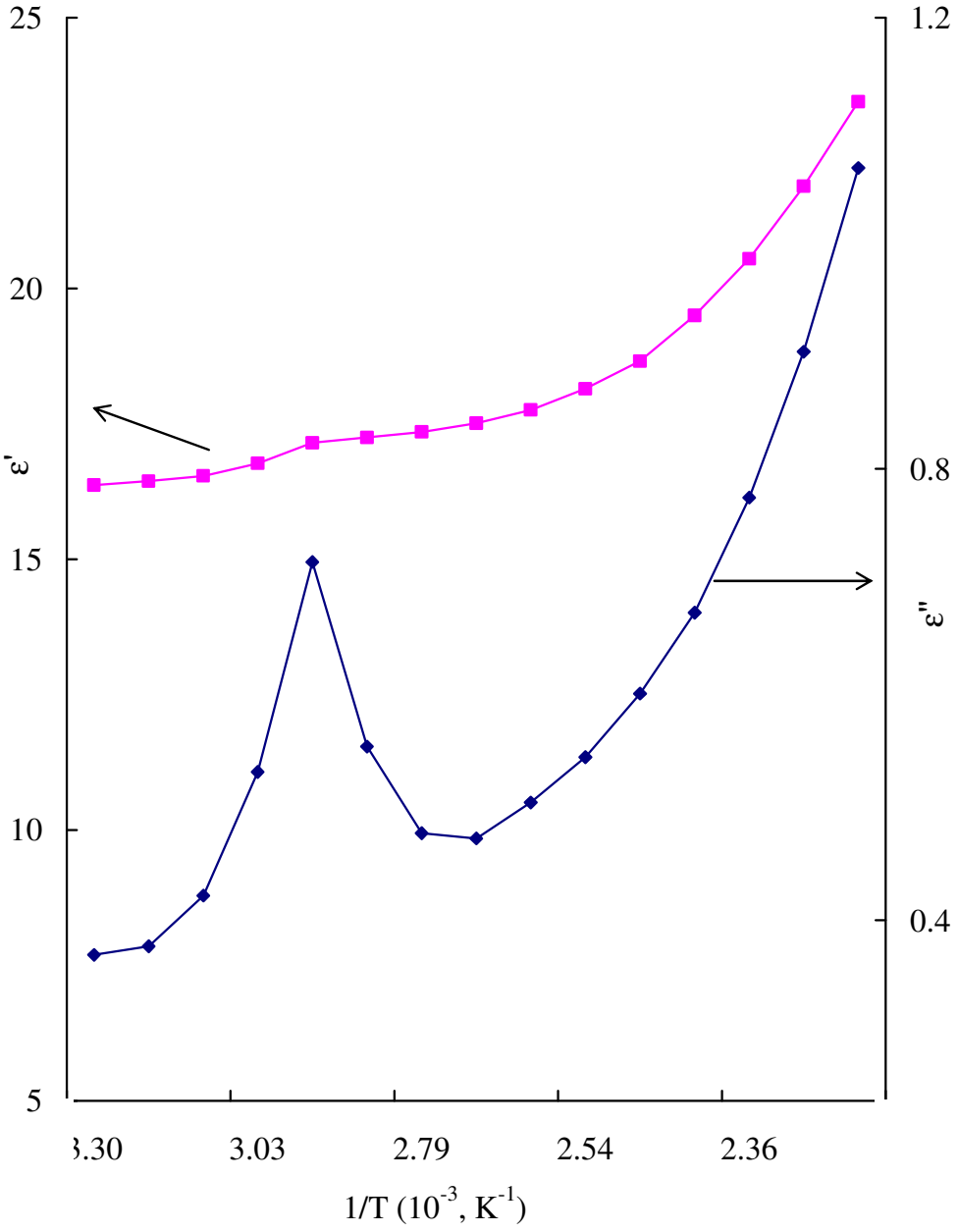

Fig. 3.15 Variation of ε'(ω, T) and ε" (ω, T) with 1/T for glass V_6.

Earlier studies on the glasses containing d^1 ions like W^{5+}, Cr^{5+}, Ti^{3+}, Mo^{5+} etc., showed that these ions contribute to the dielectric relaxation effects [88-90]; hence, in the present glasses V^{4+} ions do contribute to the relaxation effects in addition to TeO_4 structural units. The shifting of relaxation region towards lower temperatures and decrease in the activation energy with increase in the concentration of V_2O_5 from 0 to 0.6 mol% (Table 3.6) suggests an increasing degree of freedom for dipolar clusters to orient in the field direction in the glass network.

When a plot is made between log $\sigma(\omega)$ v/s activation energy for conduction (in the high temperature region) a near linear relationship is observed (inset (b) of Fig. 3.14); this observation suggests that the conductivity enhancement is directly related to the thermally stimulated mobility of the charge carriers in the high temperature region. In insulators, where broad distribution of relaxation times τ exist, like in the present samples, the ac conduction can be represented by

$$\sigma = \sigma_0 \ e^{-\xi} \qquad (3.16)$$

There are two mechanisms that could contribute to the form of Eq. (3.16) for ac conduction: the first contribution is due to the normal classical activation of a carrier over a potential barrier 'W' separating two sites, in this case ξ = W/KT. This mechanism can be adopted to the simple Debye loss case. Second contribution is due to the tunneling of a carrier through a potential barrier

between the sites separated by a distance R, in this case $\xi=2\alpha R$, where α^{-1} being the localization strength; this mechanism is applicable for explaining low-temperature part of the conductivity (nearly temperature-independent part) as described below. The way the ac conductivity varies with the temperature for the present samples indicate that both the mechanisms are responsible for ac conduction, in ZnF_2–As_2O_3–TeO_2: V_2O_5 glasses. The low temperature part of the conductivity (a near temperature independent part as in the case of present glasses) up to nearly 70 ^oC can be explained on the basis of quantum mechanical tunneling model [91] similar to many other glass systems reported recently [89, 90, 92, 93]. The value of $N(E_F)$, i.e. the density of the defect energy states near the Fermi level is evaluated at about 350 K using

$$\sigma(\omega) = \frac{\pi}{3} e^2 KT\left[NE_F\right]^2 \alpha^{-5} \omega\left[\ln\frac{\nu_{ph}}{\omega}\right]^4 \qquad (3.17)$$

where α is electronic wave function decay constant taken as 0.49 (A°) (obtained by plotting log σ_{ac} against R_i) and ν_{ph} the phonon frequency ($5x10^{12}$ Hz) and presented in Table 3.7. The value of $N(E_F)$ is found to increase with increase in the concentration of V_2O_5. Such increase also suggests an increasing disorder in the glass network with increase in the concentration of the dopant.

Our observations on dielectric parameters of ZnF_2–As_2O_3–TeO_2: V_2O_5 glasses indicated that the rate of increase of ε', tanδ (which is inversely

proportional to dielectric break down strength) with temperature is the lowest for the glass V_6. Thus the experiments on dielectric properties of ZnF_2–As_2O_3–TeO_2: V_2O_5 glasses also reveal that there is a decrease in the dielectric breakdown strength of the glasses with increase in the concentration of V_2O_5 up to 0.6 mol%. These revelations are also consistent with the view that, there is a gradual increase in the concentration of vanadyl ions, occupy modifying positions and inculcate more disorder in the glass network.

3.5 Conclusions

The summary of the results on studies of dielectric properties of ZnF_2–As_2O_3–TeO_2: V_2O_5 glasses coupled with spectroscopic studies is as follows: The optical absorption spectra of these glasses have exhibited two clearly resolved bands due to $^2B_2 \rightarrow {}^2B_1$ and $^2B_2 \rightarrow {}^2E$ transitions of vanadyl ions. The intensity and the half width of these bands have been observed to be maximal in the spectrum of glass V_6; from this observation it is concluded that VO^{2+} (vanadyl) ions present in larger concentrations in this glass network. The ESR spectra of ZnF_2–As_2O_3–TeO_2: V_2O_5 glasses recorded at room temperature are observed to be complex made up of resolved hyperfine components arising from unpaired $3d^1$ electron of ^{51}V isotope having spin 7/2. As the concentration of V_2O_5 is increased, an increase in the degree of resolution and the intensity of signal, have been observed. The quantitative analysis of the ESR spectra revealed that there is a progressive weakening of the bonding between V^{4+} ion

and equatorial oxygen as the concentration of V_2O_5 is increased. From this analysis it is also concluded that there is an increase in the degree of disorder of the octahedral and in the glass network as a whole with increase in the concentration of V_2O_5. The IR spectrum of pure glass exhibited a band due to ν_s-TeO_{2ax} (axial band) at about 643 cm^{-1} whereas the equatorial band viz., ν_s–TeO_{2eq} is observed to be missing; the spectra also exhibited bands due to ν_1 and ν_2-vibrations of AsO_3 structural groups. V_2O_5 doped glasses have exhibited two additional bands due to the vibrations of V–O–V chains. With the gradual increase in the concentration of V_2O_5, the ν_s–TeO_{2ax} and ν_2 of AsO_3 bands are shifted gradually towards considerably higher frequencies with decreasing intensity. Such changes have been understood due to increasing modifying action of vanadyl ions in the glass network with increase in the concentration of V_2O_5. The photoluminescence spectra of ZnF_2–As_2O_3–TeO_2: V_2O_5 glasses recorded at room temperature with the excitation wavelength of 640 nm exhibited a broad emission band in the region 750-850 nm due to $^2E \rightarrow {}^2T_2$ transition of vanadyl ion. With increase in the concentration of V_2O_5, the intensity of the peak is observed to increase with a red shift. The shift of this PL peak, the shape and the structured nature of the PL emission band have been identified as a signature of shallow levels with an electron–phonon coupling. The dielectric parameters viz., ε' tan δ and σ_{ac} are found to increase and the activation energy for ac conduction is found to decrease with the

increase in the concentration of V_2O_5 up to 0.6 mol%. This result point out that there is a gradual increase in the concentration of V^{4+} ions those act as modifiers in the glass network. The analysis of dielectric loss studies indicated that these glasses exhibit dipolar effects. The ac conduction could be explained both due to classical activation energy and due to the tunneling phenomena.

References

[1] B.V. Raghavaiah, N. Veeraiah, *J. Phys. Chem. Solids* 65 (2004) 1153.

[2] K. Nassau, *Bell Syst. Tech. J.* 60 (1981) 327.

[3] A. Bishay, C. Maghrabi, *Phys. Chem. Glasses* 10 (1969) 1.

[4] M.M. El-Desoky, S.M. Abo-Naf, *J. Mater. Sci.: Mater. Electron.* 15 (2004) 425.

[5] M.N. Khan, *Phys. Stat. Solidi (a)* 114 (2006) 285.

[6] B.V. Raghavaiah, C. Laxmi Kanth, D. Krishna Rao, N. Veeraiah, *Mater. Lett.* 59 (2004) 539.

[7] N. Krishna Mohan, G. Sahaya Baskaran, N. Veeraiah, *phys. stat. sol. (a)* 203 (2006) 2083.

[8] O. Cozar, I. Ardelean, V. Simon, G. Ilonca, C. Crocium, C. Cefan, *J. Alloys Compd.* 326 (2001) 124.

[9] M. Prashant Kumar, T. Sankarappa, B. Vijaya Kumar, N. Nagaraja, *Solid State Sci.* 11 (2009) 214.

[10] R. Balaji Rao and N. Veeraiah, *Physica B* 348 (2004) 256

[11] N. Kerkouri, M. Et-Tabirou, A. Chahine, A. Mazzah, M.C. Dhamelincourt, M. Taibi, *J. Optoelectr. Adv. Mater.* 12 (2010) 1030

[12] X. Lin-Hua, Z. Guo-Ping, Q. Min, *Physica B* 405 (2010) 2213.

[13] M.E. Gouda, H. Khodair, M.G. El-Shaarawy, *Mater. Chem. Phys.* 120 (2010) 608.

[14] S.A.E., Ali, F.M. Ezz-Eldin, *Nucl. Instr. Meth. Phys. Res., Sec. B* 268 (2010) 49.

[15] N.S. Abd El-Aal, H.A. Afifi, *Archiv. Acoust.* 34 (2009) 641.

[16] A. Agarwal, A. Sheoran, S. Sanghi, V. Bhatnagar, S.K. Gupta, M. Arora, *Spectrochim. Acta - Part A* 75 (2010) 964.

[17] G.D. Khattak, A. Mekki, L.E. Wenger, *J. Non-Cryst. Solids* 355 (2009) 2148.

[18] A. Mekki, G.D. Khattak, L.E. Wenger, *J. Electr. Spectr. Rel. Phen.* 175 (2009) 21.

[19] H. Behzad, M.H. Hekmatshoar, M. Mirzayi, M. Azmoonfar, *Ionics* 15 (2009) 647.

[20] Y.B. Saddeek, *Phil. Mag.* 89 (2009) 2305.

[21] M. Shapaan, E.R. Shabaan, A.G. Mostafa, *Physica B* 404 (2009) 2058.

[22] W.L. Feng, *Phil. Mag.* 89 (2009) 1391.

[23] L.D. Bogomolova, V.A. Zhachkin, T.K. Pavlushkina, *Glass Ceram.* 66 (2009) 168.

[24] Y.V. Kartashov, V.A. Vysloukh, *Opt. Lett.* 34 (2009) 1228.

[25] S.H. Kim, O.H. Han, J.P. Kang, S.K. Song, *Bull. Korean Chem. Soc.* 30 (2009) 608.

[26] W. Sung, J. Won, J. Lee, H. Kim, *Mol. Cryst. Liq. Cryst.* 499 (2009) 234.

[27] H.M.M. Moawad, H. Jain, R. El-Mallawany, *J. Phys. Chem. Solids* 70 (2009) 224.

[28] Y. Taibi, M. Poulain, R. Lebullenger, L. Atoui, M. Legouera, *J. Optoelectr. Adv. Mater.* 11 (2009) 34.

[29] F.H. ElBatal, Y.M. Hamdy, S.Y. Marzouk, *Mater. Chem. Phys.* 112 (2008) 991.

[30] H. Farah, *J. Am. Ceram. Soc.* 91 (2008) 3915.

[31] M.P. Kumar, T. Sankarappa, A.M. Awasthi, *Physica B* 403 (2008) 4088.

[32] N. Vedeanu, O. Cozar, I. Ardelean, B. Lendl, D.A. Magdas, *Vibr. Spectr.* 48 (2008) 259.

[33] V. Kundu, R.L. Dhiman, D.R. Goyal, A.S. Maan, *J. Optoelectr. Adv. Mater.* 10 (2008) 2765.

[34] L. Srinivasa Rao, M. Srinivasa Reddy, M. Rami Reddy, N. Veeraiah, *J. Alloys Compd.* 464 (2008) 472.

[35] S. Rada, M. Culea, M. Rada, E. Culea, *J. Mater. Sci.* 43 (2008) 6122.

[36] C. Li, Y. Huang, Z. Cui, X. Gao, Z. Gu, *J. Chin. Ceram. Soc.* 36 (2008) 1288.

[37] M.S. Al-Assiri, *Physica B* 403 (2008) 2684.

[38] Q.B. Tian, Y. Wang, X.T. Yue, Y.S. Yin, *Mater. Sci. Tech.* 16 (2008) 543.

[39] I.Z. Hager, *Mater. Chem. Phys.* 109 (2008) 365.

[40] I. Ardelean, O. Cozar, N. Vedeanu, D. Rusu, C. Andronache, *J. Mater. Sci.* 18 (2007) 963.

[41] A. Mekki, G.D. Khattak, D. Holland, M. Chikhota, L.E.Wenger, *J. Non-Cryst. Solids* 318 (2003) 20.

[42] A.M. Ferrari, C. Leonelli, G.C. Pellacani, C. Siligardi, *J. Non-Cryst. Solids* 315 (2003) 77.

[43] Abd EI-Moneim, *Mater. Chem. Phys.* 73 (2002) 318.

[44] U. Hoppe, E. Yousef, C. Russel, J. Neuefeind, A.C. Hannon, *Solid State Commun.,*123 (2002) 273.

[45] O. Cozar, I. Ardelean, I. Bratu, V. Simon, C. Craciun , L. David, C. Cefan, *J. Mol. Struct.* 563 (2001) 421.

[46] M.A. Salim, P.S. Fodor, L.E. Wenger, *J. Non-Cryst. Solids* 85 (2001)195.

[47] G.D. Khattak, M.A. Salim, L.E. Wenger, A.H. Gilani, *J. Non-Cryst. Solids* 262 (2000) 66.

[48] J.K. Jung, S.K. Song, T.H. Noh, O.H. Han, *J. Non-Cryst. Solids* 270 (2000) 97.

[49] K. Krasowski, M. Wasiucionek, *Phys. Stat. Solidi (a)* 181 (2000)157.

[50] Maria-Cameljaungureanu, Michri Levy, Jeal-louis Souquet, *J. Ceramics. Silikaty* 44 (2000) 81.

[51] H. Mori, H. Matsuno, H. Sakata, *J. Non-Cryst. Solids* 276 (2000) 78.

[52] V. Rajendranan, N. Palanivelu, D.K. Modak and B.K. Chaudhuri, *Phys. Stat. Solidi (a)* 180 (2000) 467.

[53] J. Simockova, P. Miklos, V. Saly, *J. Acta Phys. Slovaca,* 50 (2000) 685.

[54] V. Sudarsan, S.K. Kulshreshtha, *J. Non-Cryst. Solids* 258 (1999) 20.

[55] K. Sega, H. Kasai, H. Sakata, *Mater. Chem. Phys.* 53 (1998) 28.

[56] Y. M. Moustafa, I. A. Gohar, A. A. Megahed and E. L. Mansour, *Phys. Chem. Glasses* 38 (1997) 92.

[57] O. Attos, M. Massot, M. Aspomoza, *J. Non-Cryst. Solids* 210 (1997) 163.

[58] L. Murawski, R.J. Barczynski, *J. Non-Cryst. Solids* 196 (1996) 275.

[59] V.P. Seth, D. Prakash, P. Chand, *J. Non-Cryst. Solids* 204 (1996) 46.

[60] H. Takahashi, Y. hakai, Y. Morii, *Solid State Ionics* 90 (1996) 125.

[61] D. Prakash, V.P. Seth, I. Chand, Prem Chand, *J. Non-Cryst. Solids* 204 (1995) 46

[62] L.D. Bogomolva, N.A. Krasilnikova, V.L. Bogdanov, V.D. Khalilev, *J. Non- Cryst. Solids* 188 (1995) 130.

[63] T. Yoko, S. Hayakawa, S. Sakka, *J. Non-Cryst. Solids* 183 (1995) 73.

[64] A. Ghosh, S. Mandal, S. Hazra, D. Dass, *J. Non-Cryst. Solids* 183 (1995) 317.

[65] S. Gupta, A. Mansingh, *J. Non-Cryst. Solids* 181 (1995) 58.

[66] S. Adams, K. Hariharan, J. Maier, *Solid State Ionics* 75 (1995) 193.

[67] V. Demitrov, Y. Dimitriev, A. Montenero, *J. Non-Cryst. Solids* 180 (1994) 51.

[68] M. Amano, K. Suzuki, H. Sakata, *J. Mater. Sci.* 32 (1997) 4325.

[69] J. Ballhausen, H.B. Gray, *Inorg. Chem.* 1 (1962) 111.

[70] I. Morozova, A. Yakind, *Fis. Khim. Stekla* 3 (1977) 197.

[71] O. Miroschnichenko, O. Klimaschevski, *Neorg. Mater.* 6 (1970) 1893.

[72] Y. Dimitriev, Y. Ivanova, M. Dimitrova, *J. Mater. Sci. Lett.* 19 (2000)1513.

[73] M. Ueno, K. Suzuki, *Kakuriken Kenyo Hokoku* (Tohoku Univ.) 16 (1983) 349.

[74] A. Berthereau, Y. Le Luyer, R. Olazcuaga, *Mater. Res. Bull.* 29 (1994) 933.

[75] N. Mochida, K. Takahashi, K. Nakata, *Yogyo Kyokai Shi* 86 (1978) 316.

[76] A.G. Clare, A.C. Wright, R.N. Sinclair, A.E. Geissberger, *J. Non-Cryst. Solids* 111 (1989) 123.

[77] C.H. Chung, J.D. Mackenzie, *J. Non-Cryst. Solids* 42 (1980) 357.

[78] A.I. Nicula, E. Culea, I. Lupsa, *J. Non-Cryst. Solids* 79 (1986) 325.

[79] E.E. Metwalli, *J. Non-Cryst. Solids* 317 (2003) 22.

[80] W. Ryba-Romanowski, S. Golab, G. Dominiak-Dzik, M. Berkowski, *J. Alloys Compd.* 288 (1999) 262.

[81] G. Murali Krishna, M. Srinivasa Reddy, N. Veeraiah, *J. Solid State Chem.* 180 (2007) 2747

[82] L. Srinivasa Rao, M. Srinivasa Reddy, D. Krishna Rao, N. Veeraiah *J. Solid State Sci*. 11 (2009) 578.

[83] P. Venkateswara Rao, T. Satyanarayana, M. Srinivasa Reddy, Y. Gandhi, N. Veeraiah, *Physica B* 403 (2008) 3751.

[84] C.J.F. Bottcher, P. Bordewijk, *Thoery of Electric Polarization* (Elsevier, Oxford, 1978).

[85] R.T. Sanderson, "*Inorganic Chemistry*" Vol. 194 (Affiliated East West Press Pvt., Ltd., New Delhi, 1971).

[86] A. Singh, V. K. Dhawan, *Phil. Mag. B* 48 (1983) 215.

[87] D.K. Durga, N. Veeraiah, *J. Mater. Sci.* 36 (2001) 5625.

[88] R M Abdelouhab, R. Braunstein, K. Baernerm, *J. Non-Cryst. Solids* 108 (1989) 109.

[89] K. Sambasiva Rao, M. Srinivasa Reddy, V. Ravi Kumar, N. Veeraiah, *Mater. Chem. Phys.* 111 (2008) 283.

[90] M. Srinivasa Reddy, S.V.G.V.A. Prasad, N. Veeraiah, *Phys. Stat. Solidi (a)* 204 (2007) 816.

[91] I.G. Austin, N.F. Mott, *Adv. Phys.*18 (1969) 657.

[92] G. Sahaya Baskaran, D. Krishna Rao, N. Veeraiah, *Solid State Commun.* 145 (2008) 401.

[93] P. Venkateswara Rao, M. Srinivasa Reddy, K.S.V. Sudhakar, N. Veeraiah, *Phil. Mag.* 88 (2008) 1601.